



S(-) and R(+) species derived from antihistaminic promethazine agent: structural and vibrational studies



María Eugenia Manzur, Silvia Antonia Brandán*

Cátedra de Química General, Instituto de Química Inorgánica, Facultad de Bioquímica, Química y Farmacia, Universidad Nacional de Tucumán, Ayacucho 471, San Miguel de Tucumán, Tucumán, 4000, Argentina

ARTICLE INFO

Keywords:

Computer science
Theoretical chemistry
Electronic
Structural properties
DFT calculations
Promethazine
Descriptor properties

ABSTRACT

Structural and vibrational properties of free base, cationic and hydrochloride species derived from both S(-) and R(+) enantiomers of antihistaminic promethazine (PTZ) agent have been theoretically evaluated in gas phase and in aqueous solution by using the hybrid B3LYP/6-31G* calculations. The initial structures of S(-) and R(+) enantiomers of hydrochloride PTZ were those polymorphic forms 1 and 2 experimentally determined by X-ray diffraction. Here, all structures in aqueous solution were optimized at the same level of theory by using the polarized continuum (PCM) and the universal solvation model. As was experimentally reported, variations in the unit cell lead to slight energy, density, and melting point differences between the two forms but, this behavior is not carried through in isotropic condition, like in solution with non-chiral solvents. Hence, the N–C distances, Mulliken, atomic natural population (NPA) and Merz-Kollman (MK) charges, bond orders, stabilization and solvation energies, frontier orbitals, some descriptors and their topological properties were compared with the antihistaminic cyclizine agent. The frontier orbitals studies show that the free base species of both forms in solution are more reactive than cyclizine. Higher electrophilicity indexes are observed in the cationic and hydrochloride species of PTZ than cyclizine while the cationic species of cyclizine have higher nucleophilicity index than both species of PTZ. The presences of bands attributed to cationic species of both enantiomers are clearly supported by the infrared and Raman spectra in the solid phase. The expected 114, 117 and 120 vibration normal modes for the free base, cationic and hydrochloride species of both forms were completely assigned and the force constants reported. Reasonable concordances among the predicted infrared, Raman, UV-Vis and Electronic Circular Dichroism (ECD) with the corresponding experimental ones were found.

1. Introduction

Species containing in their structures the N–CH₃ group presenting a wide range of pharmacological and medicinal properties such as tropane alkaloids whose known biological effects can cause from pain cure up to addiction [1, 2, 3, 4, 5, 6, 7]. However, there are another groups of species that also contain that group but that present other different biological properties such as, diphenhydramine and cyclizine, where both species are broadly used in pharmacology as antihistaminic agents [8, 9]. Nevertheless, the most remarkable differences among the free base, cationic and hydrochloride species of those two antihistaminic agents are that in the species derived from diphenhydramine their two N–CH₃ groups are not linked to rings while in the cyclizine species those groups are linked to piperazine rings [8, 9]. Previous theoretical studies on structures and properties of alkaloids have evidenced that when the

N–CH₃ group is linked to fused rings as in scopolamine, cocaine and tropane some properties are slightly different from those where the N–CH₃ group is linked to only one ring as in heroin and morphine [1, 2, 3, 5, 6, 7]. Besides, the stabilities of these series of alkaloids are strongly dependent on the N–C distances [6, 7]. On the other hand, the reactivities predicted for the three species of diphenhydramine practically are the same than that reported for cationic form of cocaine [3, 7] while lowest solvation energy value was observed for the free base of cyclizine, as compared with the corresponding to tropane alkaloids [9]. Evidently, there is an important connection between the quantity of N–CH₃ groups and the type of groups linked to N atom, that is, >N- tertiary or >N< quaternary. Consequently, the biological activities and effects of these types of species on human health are obviously resulted of their nature and structural, electronic and topological properties. Hence, the interest to study another antihistaminic agent, in this case promethazine (PTZ)

* Corresponding author.

E-mail address: sbrandan@fbqf.unt.edu.ar (S.A. Brandán).

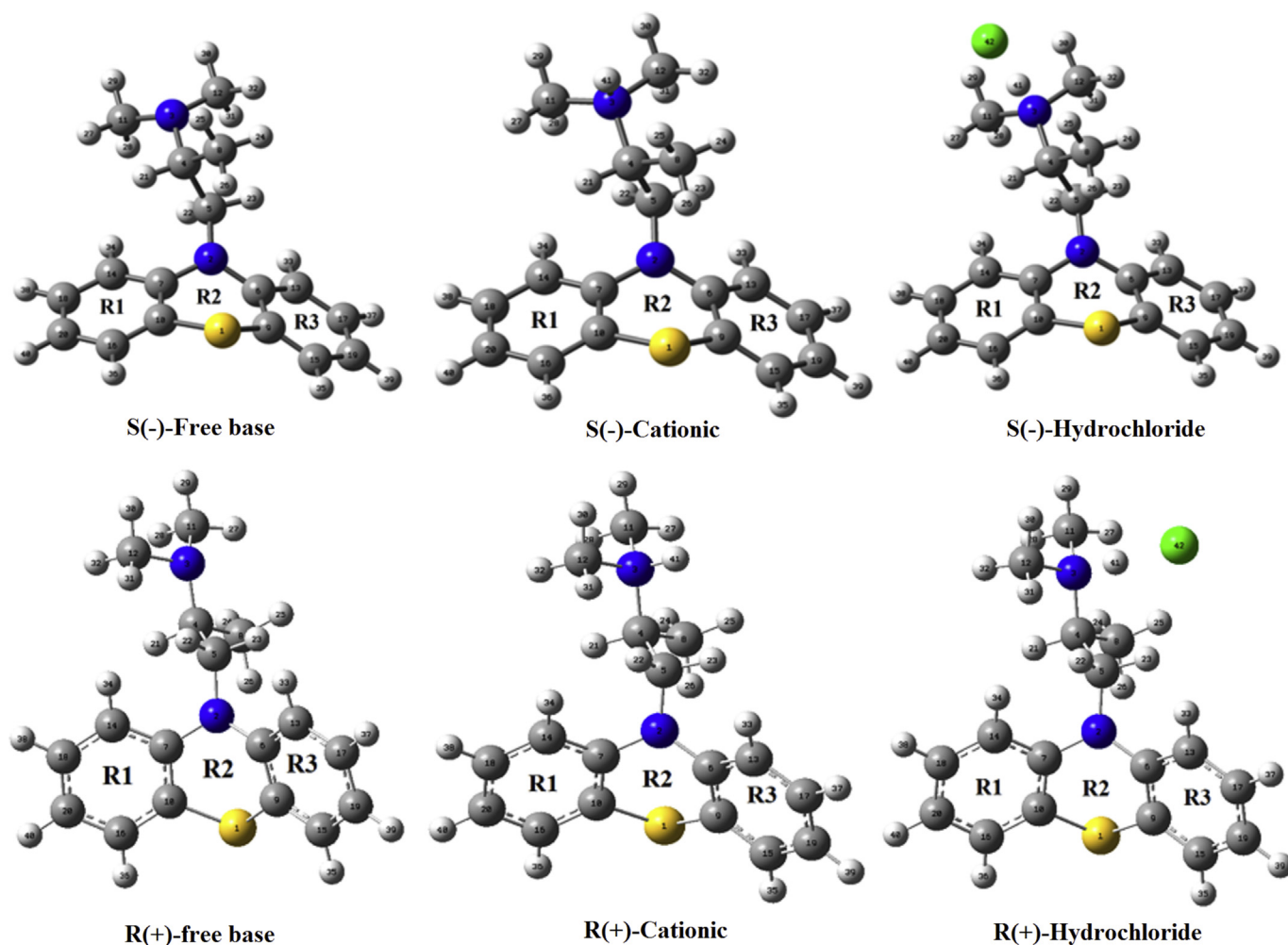


Fig. 1. Theoretical molecular structures of free base, cationic and hydrochloride species of both S(-) and R(+) enantiomers of promethazine.

Table 1

Calculated total energies (E), dipole moments (μ) and volumes (V) of three species of S(-) and R(+)-promethazine in gas and aqueous solution phases.

B3LYP/6-31G* Method				
Medium	E (Hartrees)	ZPVE	μ (D)	V (\AA^3)
S(-)-Free base				
GAS	-1167.5298	-1167.1923	2.18	312.7
PCM	-1167.5383	-1167.2000	3.75	314.2
S(-)-Cationic				
GAS	-1167.9143	-1167.5615	14.62	316.3
PCM [#]	-1167.9121	-1167.5588	15.20	315.1
S(-)-Hydrochloride				
GAS	-1628.3493	-1627.9992	9.33	342.1
PCM	-1628.3849	-1628.0312	14.16	342.8
R(+)-Free base				
GAS	-1167.5263	-1167.1907	1.92	312.3
PCM	-1167.5277	-1167.1894	3.03	312.2
R(+)-Cationic				
GAS	-1167.9127	-1167.5599	14.77	315.9
PCM	-1168.0075	-1167.6532	19.73	319.0
R(+)-Hydrochloride				
GAS	-1628.3509	-1628.0002	7.50	338.6
PCM	-1628.3836	-1627.9920	11.72	341.4

[#] Imaginary frequencies.

[10, 11, 12, 13, 14, 15, 16, 17, 18, 19, 20, 21, 22, 23, 24, 25, 26, 27, 28, 29, 30, 31, 32, 33], which has two N-CH₃ groups (as diphenhydramine) linked to a chiral carbon and, as a consequence two enantiomeric S and R structures are expected for their three free base, cationic and hydrochloride species. PTZ hydrochloride is a drug used to treatment of nausea, vomiting, and dizziness associated with motion sickness and, besides possesses anti-pruritic, anti-allergic, anticholinergic, antihistaminic, central nervous system depressant, and with general anaesthetics effects. Their metabolic and clinic effects were studied from long time together with their side effects [13, 29, 30, 31, 32, 33]. Some known chemical names of promethazine are proazamine, diphergan, phenargan or phensedyl while its IUPAC name is N,N-dimethyl-1-phenothiazin-10-ylpropan-2-amine. PTZ has structurally two >N-CH₃ groups, three fused six members rings (two phenyl and one phenothiazine) and a chiral carbon and where experimentally Borodi et al [19] have determined by X-ray diffraction two enantiomeric disordered structures of promethazine hydrochloride but, so far, the structural properties and vibrational assignments of those three species of PTZ were not published. The vibrational analyses of the three species of PTZ are actually of great interest and significance taking into account that the infrared, Raman and SERS spectroscopies are practically the most used spectroscopic techniques to identify these species in different systems and preparations [10, 12, 15, 17, 22, 23, 24, 25, 26, 27, 28]. Hence, the aims of this work are: (i) to study the structural, electronic, topological and vibrational properties of free base, cationic and hydrochloride species of S(-) and R(+)-PTZ, (ii) to find some correlations between their properties that can explain the differences between its biological properties, as compared

Table 2

Corrected and uncorrected solvation energies by the total non-electrostatic terms and by zero point vibrational energy (ZPVE) of three species of S(-) and R(+)-promethazine by using the B3LYP/6-31G* method compared with other similar species.

B3LYP/6-31G* method ^a			
Solvation energy (kJ/mol)			
Condition	$\Delta G_{un}^{\#}$	ΔG_{ne}	ΔG_c
Free base			
S(-)-Promethazine ^a	-20.19	15.88	-36.07
R(+)-Promethazine ^a	-3.41	14.46	-17.87
Cyclizine ^b	-23.60	5.93	-29.53
Morphine ^c	-47.74	13.17	-60.91
Cocaine ^d	-42.75	28.51	-71.26
Scopolamine ^e	-56.66	18.81	-75.47
Heroin ^f	-59.54	29.13	-88.67
Tropane ^{g,s}	-11.80	0.75	-12.55
Cationic			
S(-)-Promethazine ^a	-7.08	7.40	-14.48
R(+)-Promethazine ^a	-255.22	7.59	-262.81
Cyclizine ^{b,#}	-238.43	5.93	-244.36
Morphine ^c	-282.23	26.96	-309.19
Cocaine ^d	-216.66	38.58	-255.24
Scopolamine ^e	-279.87	30.47	-310.34
Heroin ^f	-280.13	43.01	-323.14
Tropane ^{g,s}	-228.99	15.34	-244.33
Hydrochloride			
S(-)-Promethazine ^a	-101.25	30.81	-70.44
R(+)-Promethazine ^a	-21.51	30.51	-52.02
Cyclizine ^b	-81.57	23.49	-105.06
Morphine ^c	-118.82	25.92	-144.74
Cocaine ^d	-99.94	38.20	-138.14
Scopolamine ^e	-95.19	27.55	-122.74
Heroin ^f	-118.56	43.38	-161.94
Tropane ^{g,s}	-72.13	15.05	-87.18

$\Delta G_{un}^{\#}$ = uncorrected solvation energy: defined as the difference between the total energies in aqueous solutions and the values in gas phase. ΔG_{un} = Solvation energy (kJ/mol) corrected by ZPVE.

ΔG_{ne} = total non electrostatic terms: due to the cavitation, dispersion and repulsion energies.

ΔG_c = corrected solvation energies: defined as the difference between the uncorrected and non-electrostatic solvation energies.

^a This work.

^b From Ref [9].

^c From Ref [1].

^d From Ref [3].

^e From Ref [7].

^f From Ref [5].

^g From Ref [2].

[#] Cation cyclizine: 6-31+G*.

with alkaloids and other antihistaminic agents, (iii) to perform the complete vibrational assignments of those three species of PTZ because, so far, these are not reported. In accordance to previous studies, the infrared spectra of many hydrochloride species show clearly the presence of their cationic forms in the solid phase and in aqueous solution [1, 2, 3, 5, 7, 8]. To achieve those purposes, the theoretical structures of free base, cationic and hydrochloride species of both S(-) and R(+)-PTZ enantiomers were optimized in gas phase and in aqueous solution by using the hybrid B3LYP/6-31G* method [34, 35] while experimental infrared and Raman spectra available from the literature were used to perform the vibrational analyses [17, 24, 25, 26, 27, 28]. The studies in solution were performed with the integral equation formalism variant polarised continuum method (IEFPCM) because it scheme contemplates the solvent effects while the solvation energies were computed with the universal solvation model [36, 37, 38]. Hence, for those three S(-) and R(+)-PTZ species, atomic charges, molecular electrostatic potential, bond orders, frontier orbitals and topological properties were calculated together with

the harmonic force fields by using the scaled quantum mechanical force field (SQMFF) and transferable scaling factors [39, 40]. Then, the complete assignments for the three species were performed by using the corresponding force fields, internal normal coordinates and the experimental available vibrational spectra of PTZ hydrochloride [41] together with the Molvib program [42]. Taking into account the wide range of biological activities that presents PTZ, the reactivities and behaviours of those three S(-) and R(+)-PTZ species were predicted in both media by using the frontier orbitals [43, 44] and global descriptors [45, 46, 47, 48, 49, 50, 51, 52, 53]. Finally, the predicted properties of both enantiomeric series of S(-) and R(+)-PTZ were evaluated and then compared with the available data reported for alkaloids, diphenhydramine and cyclizine [1, 2, 3, 4, 5, 6, 7, 8, 9].

2. Methodology

2.1. Ab-initio calculations

The initial structure of S(-) enantiomer of PTZ hydrochloride was that experimental polymorphic form 1 determined by X-ray diffraction by Borodi et al [19] and taken from the available CIF file. The corresponding cationic and free base species were modelled respectively by using the GaussView program [54] where the Cl atom was first removed from that initial structure of PTZ hydrochloride and, later, the H atom. A similar procedure was employed to obtain the three species of R(+) enantiomer but in this case the structures were built from that experimental polymorphic form 2 determined by X-ray diffraction by Borodi et al [19]. The Revision A.02 of Gaussian program was employed to optimize those six species in both media [55] by using the hybrid B3LYP/6-31G* method [34, 35]. In solution, the three species were optimized by using PCM and SMD calculations [36, 37, 38] while their volumes changes were evaluated with the Moldraw program [56]. In Fig. 1 can be seen the six S(-) and R(+)-PTZ structures as free base, cationic and hydrochloride together with the atoms labelling and the identifications of their three rings. The solvation energies corrected by zero point vibrational energy (ZPVE) were computed for all species of S(-) and R(+)-PTZ with the universal solvation model [36, 37, 38]. Besides, atomic natural population (NPA), Mulliken and Merz-Kollman (MK) charges [57], molecular electrostatic potentials, bond orders and topological properties were calculated by using the NBO program [58] and with the Bader's theory of atoms in molecules (AIM) by using AIM2000 program [59, 60]. On the other hand, the evaluation of reactivities and behaviours of S(-) and R(+)-PTZ species were performed calculating the gap values [43, 44] and some useful and known global descriptors with the frontier orbitals [45, 46, 47, 48, 49, 50, 51, 52, 53]. The harmonic force fields and force constants in gas phase and in aqueous solution were computed at the B3LYP/6-31G* level by using the normal internal coordinates and transferable scaling factors with the scaled quantum mechanical force field (SQMFF) and the Molvib program [39, 40, 42]. Here, the predicted Raman activities for all species were corrected to intensities by using recommended equations [61, 62] while the scale factors used were those reported for the B3LYP/6-31G* method. At this point, it is necessary to clarify that all studied properties were computed for six S(-) and R(+)-PTZ species by using only the B3LYP/6-31G* level because they are compared with properties reported at the same level of theory for other species containing N-CH₃ groups, such as alkaloids, diphenhydramine and cyclizine [1, 2, 3, 6, 7, 8, 9].

3. Results and discussion

3.1. Properties of species of S(-) and R(+)-PTZ in both media

The structural studies in solution of these species are of great interest because the >N-CH₃ group can present fast N-methyl inversion in this medium, as suggested by Lazni et al [63]. Here, in Table 1 are summarized calculated total uncorrected and corrected by ZPVE energies, dipole moments and volumes (V) of three species of both enantiomers S(-) and

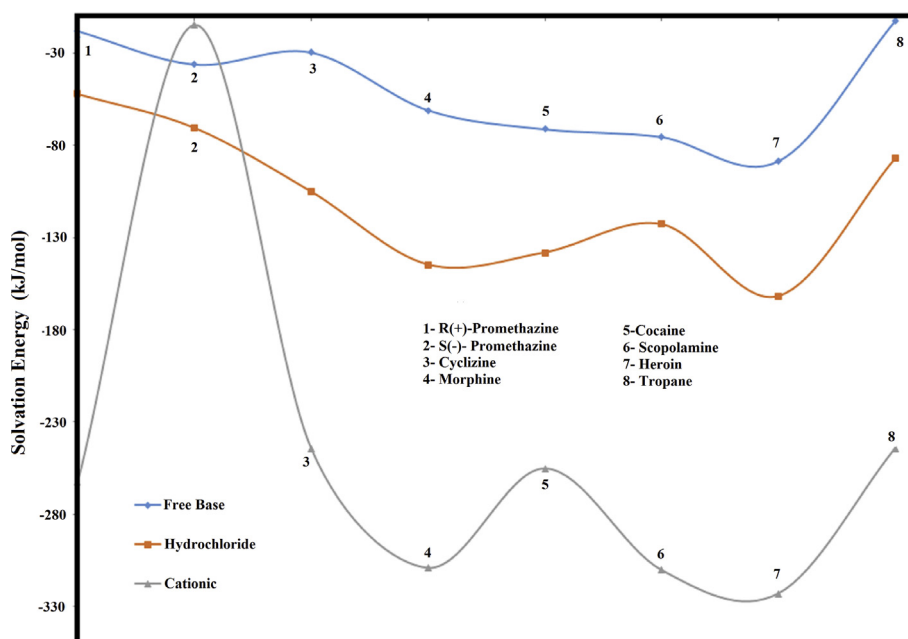


Fig. 2. Corrected solvation energies of free base, cationic and hydrochloride species of both S(-) and R(+) enantiomers of promethazine by using the B3LYP/6-31G* method.

R(+)-PTZ in gas and aqueous solution phases by using the B3LYP/6-31G* method. Analyzing deeply the results, it is observed that the total energy values corrected by ZPVE decrease for all species in both media while the dipole moment and volume values increase in solution, as expected because these species are possibly hydrated in solution. The exception is observed only for the cationic form of S(-)-PTZ because the E and V values decrease in solution. Here, the imaginary frequencies obtained for that species could justify clearly these differences. Note that the cationic species of both enantiomers have higher dipole moments in solution while the hydrochloride forms present the higher volumes in both media having the S(-) species slightly the higher values in the two media. In Table 2 can be observed corrected and uncorrected solvation energies by the total non-electrostatic terms and by zero point vibrational energy (ZPVE) of free base, cationic and hydrochloride species of S(-) and R(+)-PTZ by using the B3LYP/6-31G* method. The variations observed experimentally in the unit cell lead to small displacements of the molecules in the crystal structures and, consequently, to slight energy, density, and melting point differences between the forms. Note that these obtained values are closer to those observed in the study of interaction of gelatin with promethazine hydrochloride [64]. These values are compared in the same table with morphine, cocaine, scopolamine, heroin and tropane alkaloids and with cyclizine [1, 2, 3, 4, 5, 6, 7, 9]. In particular, due to the imaginary frequencies predicted for the cationic form of cyclizine in solution the value for cyclizine was obtained by using B3LYP/6-31+G* calculations while for S(-)-PTZ in solution the value of -14,48 kJ/mol was obtained directly from Table 1. The ΔG_c values for the three species of tropane were calculated in this work. Fig. 2 shows clearly the variations of ΔG_c for all compared species by using the solvation model [38]. In general, it is observed that all cationic species have more negative values while the free bases the less negative values. The cationic forms of morphine, scopolamine and heroin have the most negative values while the S(-) form of PTZ the most low ΔG_c value. Probably, this resulted change if other basis set is used. Interesting results are observed for cyclizine (-244,36 kJ/mol) and tropane (-244,33 kJ/mol) because their cationic forms have practically the same values. In both species, the N-CH₃ groups are linked to rings, in cyclizine to piperazine ring while in tropane a two fused piperidine and pyrrolidine rings. The heroin hydrochloride species present the most negative ΔG_c value while the R(+)-PTZ the lower value. On the other hand, the free base of heroin

presents the most negative ΔG_c value while the tropane species the lowest value. Evidently, the acetyl groups in heroin increase the solvation energies of their three species, as compared with morphine. Obviously, these comparisons show easily why the hydrochloride species are highly used in pharmacology, as compared with their free base and cationic ones. Besides, the hydrochloride species in solution are in their cationic forms and show clearly high solubility in this medium. Evidently, the solubility limits visibly the drug absorption, as mentioned by Bohloko studying the formulation of an intranasal dosage form for cyclizine hydrochloride [65].

3.2. Geometries of species of S(-) and R(+)-PTZ in both media

Calculated geometrical parameters for three species of S(-) and R(+)-PTZ in both media are compared with the corresponding experimental polymorphic forms 1 and 2 [19] in Tables 3 and 4, respectively by using the root-mean-square deviation (RMSD) values. Despite theoretical B3LYP/6-31G* calculations show visibly overestimated values, as compared with the corresponding experimental ones, the results for all species of S(-)-PTZ forms show very good correlations for bond lengths (0.020–0.012 Å) but the three species of R(+)-PTZ evidence the better correlations for bond (1.7–1.3°) and dihedral angles (6.1–3.7°) than the S(-) ones. On the other hand, the higher differences in dihedral angles are predicted for the three species of S(-) form (176.1–137.9°), as can be seen in Table 3. Here, it is necessary to remember that those two polymorphic conformations found by Borodi et al [19] are experimentally the same where the two forms are present in the unit cell but our theoretical calculations show slight differences in the dihedral angles of both S(-) and R(+)-PTZ forms. Thus, the calculated bonds N2–C6 and N2–C7 lengths of phenothiazine rings belong to the three species of both S(-) and R(+)-enantiomers are practically predicted with same values but different from the bond N2–C5 lengths of side chain. In the same way, the calculated S1–C9 bonds of phenothiazine rings are approximately the same than the S1–C10 bonds while the predicted N3–C11 bonds are practically the same than the N3–C12 bonds. The predicted values for both pairs bonds are different from the corresponding experimental ones.

Another interesting comparisons are observed in the average bond N–C lengths of the N–CH₃ groups belonging to the three species of S(-) and R(+)-PTZ with those observed for cyclizine, morphine, heroin,

Table 3

Comparison of calculated geometrical parameters for three species of S(-)-promethazine in both media with the corresponding experimental ones.

Parameter	B3LYP/6-31G* Method ^a					Form 1 Experimental ^b
	Free base		Cation	Hydrochloride		
	Gas	PCM	Gas	Gas	PCM	
Bond lengths (Å)						
S1–C9	1.783	1.786	1.786	1.783	1.786	1.772
S1–C10	1.783	1.786	1.785	1.784	1.786	1.781
N2–C5	1.464	1.471	1.445	1.457	1.465	1.435
N2–C6	1.416	1.419	1.427	1.420	1.420	1.422
N2–C7	1.416	1.418	1.424	1.420	1.419	1.418
C6–C9	1.406	1.409	1.404	1.407	1.408	1.379
C7–C10	1.406	1.409	1.406	1.407	1.409	1.389
C4–C5	1.553	1.552	1.547	1.545	1.543	1.545
N3–C4	1.472	1.482	1.550	1.511	1.525	1.513
N3–C11	1.454	1.463	1.505	1.485	1.495	1.502
N3–C12	1.456	1.465	1.505	1.484	1.495	1.491
C6–C13	1.401	1.405	1.399	1.402	1.404	1.398
C9–C15	1.392	1.392	1.395	1.395	1.396	1.394
C13–C17	1.393	1.396	1.396	1.395	1.396	1.396
C15–C19	1.393	1.396	1.395	1.395	1.396	1.392
C17–C19	1.391	1.391	1.394	1.393	1.395	1.366
C7–C14	1.401	1.404	1.400	1.402	1.404	1.402
C14–C18	1.393	1.396	1.397	1.396	1.396	1.387
C16–C10	1.392	1.395	1.395	1.394	1.395	1.394
C16–C20	1.393	1.396	1.395	1.395	1.396	1.382
C18–C20	1.391	1.395	1.394	1.393	1.394	1.379
RMSD^b	0.020	0.019	0.014	0.012	0.013	
Bond angles (°)						
C9–S1–C10	97.8	97.8	98.2	98.0	98.0	96.4
C6–C9–S1	118.6	118.5	118.8	118.7	118.6	119.0
C7–C10–S1	118.6	118.5	118.7	118.6	118.6	117.9
C5–N2–C6	119.5	118.7	120.2	119.5	119.0	118.9
C5–N2–C7	119.3	119.2	119.8	119.6	119.3	119.1
C6–N2–C7	117.5	117.0	118.3	117.9	117.7	115.6
N2–C5–C4	112.7	113.2	108.6	111.3	110.6	108.9
C5–C4–N3	113.1	113.0	111.8	111.6	111.1	106.9
C4–N3–C11	114.3	112.4	113.1	114.3	113.2	111.7
C4–N3–C12	116.2	114.1	114.4	115.8	114.9	112.1
C11–N3–C12	111.9	109.8	111.2	111.2	110.7	111.4
N2–C7–C14	122.5	122.5	122.6	122.5	122.5	122.4
N2–C6–C13	122.6	122.6	122.5	122.6	122.5	121.9
S1–C10–C16	120.4	120.3	120.8	120.6	120.3	120.0
S1–C9–C15	120.4	120.3	120.7	120.5	120.3	120.0
RMSD^b	2.4	2.1	1.8	2.0	1.6	
Dihedral angles (°)						
C11–N3–C4–C5	75.9	72.8	75.7	71.0	73.8	167.0
C12–N3–C4–C5	-56.6	-53.1	-53.0	-60.3	-54.9	-67.0
N3–C4–C5–N2	-168.3	-167.7	-165.4	-169.6	-165.2	175.4
C4–C5–N2–C6	-137.3	-142.2	-127.8	-135.3	-136.5	-68.6
C4–C5–N2–C7	63.8	63.4	66.3	64.2	66.2	140.3
C14–C7–N2–C6	-135.8	-134.5	-134.5	-135.2	-136.0	-129.1
C15–C9–S1–C10	-144.8	-144.5	-144.2	-144.7	-144.8	-139.1
C8–C4–C5–N2	65.1	66.0	69.7	64.9	70.4	-65.9
RMSD^b	138.9	139.5	137.9	176.1	223.0	

The letters bold indicated RMSD values.

^a This work.^b Ref [19].

cocaine, scopolamine and tropane where the results in gas phase and in aqueous solution by using B3LYP/6-31G* calculations can be seen in Table 5. Here, due to the presence of two N–CH₃ groups the average of N–C distances between both groups were considered. In Fig. 3 are easily observed the behaviours of N–C distances of all compared species in both media. In gas phase, the comparisons between the free base and cationic species show that cationic form of cyclizine has the lowest value (1.453 Å) while the highest value is observed in the cationic species of R(+)-PTZ (1.508 Å). In solution, it is observed that the free base species have low values and different from the hydrochloride ones. Evidently, the presence of charged cationic species and electronegative Cl atoms in all

hydrochloride species produce increase in the N–C distances. The tropane hydrochloride has the shorter value while the species corresponding to R(+)-PTZ the higher value.

3.3. Atomic charges, molecular electrostatic potentials and bond orders

Mulliken, Merz-Kollman (MK) and atomic natural population (NPA) charges, molecular electrostatic potentials (MEP) and bond orders (BO), expressed as Wiberg indexes were calculated for the three forms of S(-) and R(+)-PTZ in gas phase and in aqueous solution by using B3LYP/6-31G* calculations. The resulted only for the S1, N2, N3, C8, C11 and

Table 4

Comparison of calculated geometrical parameters for three species of R(+)-promethazine in both media with the corresponding experimental ones.

B3LYP/6-31G* Method ^a							Form 2 Experimental ^b
Parameter	Free base		Cation		Hydrochloride		
	Gas	PCM	Gas	PCM	Gas	PCM	
Bond lengths (Å)							
S1–C9	1.783	1.785	1.786	1.785	1.784	1.785	1.772
S1–C10	1.783	1.786	1.785	1.786	1.782	1.785	1.781
N2–C5	1.464	1.470	1.443	1.462	1.457	1.464	1.435
N2–C6	1.418	1.418	1.427	1.420	1.423	1.421	1.422
N2–C7	1.417	1.418	1.425	1.420	1.418	1.421	1.418
C6–C9	1.408	1.409	1.404	1.408	1.407	1.409	1.379
C7–C10	1.408	1.409	1.406	1.408	1.409	1.409	1.389
C4–C5	1.551	1.549	1.554	1.547	1.552	1.548	1.545
N3–C4	1.479	1.486	1.551	1.533	1.520	1.527	1.513
N3–C11	1.460	1.468	1.508	1.502	1.487	1.496	1.502
N3–C12	1.460	1.468	1.508	1.503	1.486	1.496	1.491
C6–C13	1.403	1.404	1.399	1.403	1.402	1.404	1.398
C9–C15	1.394	1.395	1.395	1.396	1.395	1.395	1.394
C13–C17	1.395	1.396	1.396	1.396	1.395	1.396	1.396
C15–C19	1.395	1.396	1.395	1.396	1.395	1.395	1.392
C17–C19	1.393	1.395	1.394	1.395	1.393	1.394	1.366
C7–C14	1.403	1.404	1.400	1.403	1.403	1.403	1.402
C14–C18	1.395	1.396	1.397	1.396	1.396	1.396	1.540
C16–C10	1.394	1.395	1.395	1.395	1.394	1.395	1.540
C16–C20	1.395	1.396	1.396	1.396	1.395	1.396	1.540
C18–C20	1.393	1.395	1.394	1.394	1.393	1.394	1.325
RMSD^b	0.060	0.059	0.058	0.015	0.058	0.058	
Bond angles (°)							
C9–S1–C10	97.8	97.8	98.2	98.0	98.0	98.0	96.4
C6–C9–S1	118.6	118.5	118.7	118.6	118.8	118.7	119.0
C7–C10–S1	118.6	118.4	118.7	118.6	118.7	118.7	117.9
C5–N2–C6	119.2	119.3	120.0	118.9	119.1	118.7	118.9
C5–N2–C7	119.4	119.1	119.7	119.2	119.4	119.1	119.1
C6–N2–C7	117.6	117.3	118.2	117.8	118.0	117.6	115.6
N2–C5–C4	113.1	112.4	109.5	111.2	110.9	111.2	108.9
C5–C4–N3	107.7	109.1	109.4	108.2	108.6	108.6	106.9
C4–N3–C11	114.8	111.9	113.6	113.5	114.5	113.5	112.1
C4–N3–C12	111.9	110.5	112.8	112.8	113.2	112.7	111.7
C11–N3–C12	108.9	107.2	109.2	108.8	109.6	108.9	111.4
N2–C7–C14	122.5	122.5	122.7	122.5	122.6	122.5	122.4
N2–C6–C13	122.5	122.6	122.6	122.5	122.5	122.5	121.9
S1–C10–C16	120.4	120.3	120.8	120.3	120.5	120.2	121.0
S1–C9–C15	120.4	120.3	120.8	120.3	120.3	120.1	120.0
RMSD^b	1.6	1.7	1.4	1.3	1.4	1.3	
Dihedral angles (°)							
C11–N3–C4–C5	157.1	165.9	165.5	164.2	160.7	163.5	167.0
C12–N3–C4–C5	-77.8	-74.4	-69.3	-71.2	-72.5	-71.9	-67.0
N3–C4–C5–N2	172.2	165.7	170.5	171.6	171.4	166.4	175.4
C4–C5–N2–C6	137.0	136.7	130.3	137.3	133.5	137.6	139.9
C4–C5–N2–C7	-64.6	-66.7	-65.9	-65.5	-67.5	-66.7	-69.0
C14–C7–N2–C6	135.9	135.5	134.3	136.0	136.5	136.0	131.7
C15–C9–S1–C10	144.6	144.1	144.1	144.7	144.7	144.8	140.1
C8–C4–C5–N2	-64.5	-71.0	-65.8	-65.7	-65.9	-70.7	-62.7
RMSD^b	6.1	5.8	4.6	3.7	4.8	5.4	

The letters bold indicated RMSD values.

^a This work.^b Ref [19].

C12 atoms can be seen in Table 6 because these atoms present the higher variations in all species while the behaviours of MK charges on these atoms are represented in Fig. 4. Analyzing first the MK charges for the free base species of S(-) and R(+)-PTZ we observed from Fig. 4 that: (i) the MK charges on the N2, C8 and C11 atoms of all free base species undergoes important changes, presenting the highest change on N2 of free base of R(+)-PTZ in solution and (ii) the charges on the S1, N3 and C12 atoms of all species in both media have practically the same values. In the cationic species, the lower MK charges values are observed on those five atoms of S(-)-PTZ in gas phase while on N2 atoms of R(+)-PTZ species in the two media are observed the higher changes. Different behaviours are observed on the MK charges of those five atoms corresponding to the hydrochloride species in both media. Hence, the charges

on the N3 atoms have the higher values, as expected due to the presences in these species of electronegative Cl atoms. The Mulliken charges on those five atoms of free base species show practically the same behaviours but, in particular, on the N2 and C8 atoms are observed the most negative values while the NPA charges on C8 atoms of free base, cationic and hydrochloride species show the lower values in both enantiomers. The Mulliken charges in the cationic and hydrochloride species present basically the same behaviours but on the N2 atoms are observed the lower values.

The bond orders (BO) expressed as Wiberg indexes in the three species of both enantiomers in the two media have approximately the same values and behaviours, observing the higher values in the C8, C11 and C12 atoms and the lower values in the S1 atoms. In general, higher values

Table 5

Bond lengths observed between the N and C atoms of the N-CH₃ bonds belonging to the three S(-) and R(+)-promethazine species in gas phase and in aqueous solution by using B3LYP/6-31G* calculations.

Species	N-CH ₃ bonds (Å)					
	Gas phase			Aqueous solution		
	Free base	Cationic	Hydrobromide	Free base	Cationic	Hydrobromide
R(+)-promethazine ^γ	1.460	1.508	1.487	1.468	1.501	1.496
S(-)-Promethazine ^γ	1.455	1.505	1.485	1.464	#	1.495
Cyclizine	1.453	1.453	#	1.459	#	1.489
Scopolamine	1.462	1.492	1.491	1.466	1.491	1.493
Heroin	1.453	1.501	1.483	1.460	1.498	1.492
Morphine	1.453	1.500	1.483	1.460	1.497	1.493
Cocaine	1.459	1.493	1.487	1.467	1.492	1.494
Tropane	1.458	1.496	1.478	1.467	1.491	1.486

Imaginary frequencies.

^γ average.

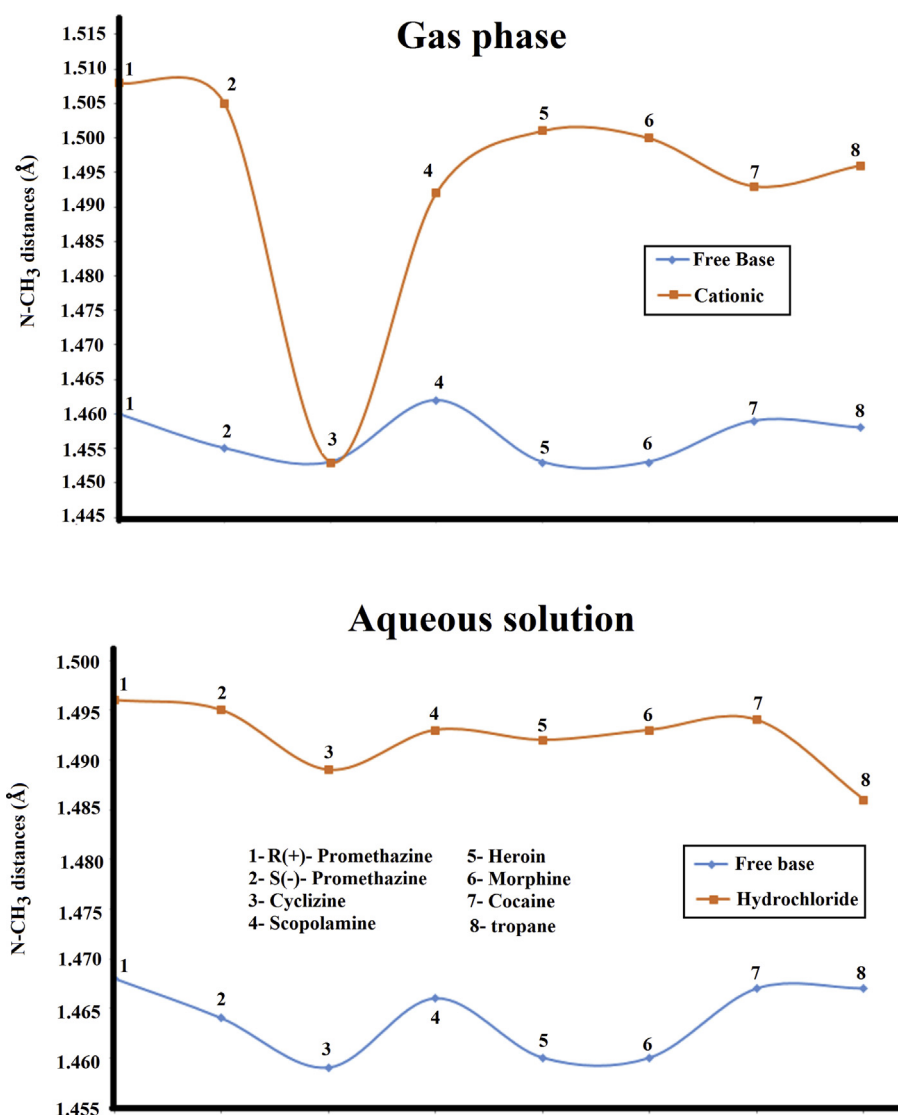


Fig. 3. Calculated N-C distances corresponding to N-CH₃ groups of free base, cationic and hydrochloride species of both S(-) and R(+) enantiomers of promethazine in both media by using the B3LYP/6-31G* method.

are observed for the N2 atoms of the free base and hydrochloride species of both S(-) and R(+)-PTZ in the two media than for the N3 atoms and only in the cationic species are observed higher values in the N3 atoms.

The molecular electrostatic potentials (MEP) presented in Table 6

show practically the same values and behaviours in the three species of both enantiomers, however, when the surfaces of these species are mapped the colorations show important differences among them, as can be seen in Fig. 5. Thus, the cationic species of both enantiomers in gas

Table 6

Mulliken, Merz-Kollman and NPA charges, molecular electrostatic potentials (MEP) and bond orders, expressed as Wiberg indexes for three forms of S(-) and R(+)-promethazine in gas phase and in aqueous solution by using B3LYP/6-31G* calculations.

S(-)-Free base										
GAS						PCM				
Atoms	MK	Mulliken	NPA	MEP	BO	MK	Mulliken	NPA	MEP	BO
S1	-0.120	0.157	0.330	-59.182	2.335	-0.118	0.156	0.328	-59.182	2.333
N2	-0.311	-0.581	-0.452	-18.312	3.305	-0.360	-0.581	-0.449	-18.311	3.305
N3	-0.346	-0.365	-0.506	-18.356	3.127	-0.357	-0.367	-0.501	-18.354	3.115
C8	-0.272	-0.455	-0.685	-14.757	3.844	-0.267	-0.455	-0.685	-14.756	3.844
C11	-0.222	-0.300	-0.468	-14.719	3.819	-0.266	-0.305	-0.473	-14.719	3.820
C12	-0.138	-0.308	-0.475	-14.719	3.819	-0.124	-0.311	-0.479	-14.720	3.820
S(-)-Cationic										
GAS						PCM				
Atoms	MK	Mulliken	NPA	MEP	BO	MK	Mulliken	NPA	MEP	BO
S1	-0.097	0.186	0.348	-59.085	2.343					
N2	-0.122	-0.587	-0.471	-18.197	3.264					
N3	-0.025	-0.492	-0.450	-18.052	3.469					
C8	-0.279	-0.498	-0.718	-14.593	3.809					
C11	-0.335	-0.348	-0.475	-14.519	3.713					
C12	-0.368	-0.351	-0.479	-14.519	3.715					
S(-)-Hydrochloride										
GAS						PCM				
Atoms	MK	Mulliken	NPA	MEP	BO	MK	Mulliken	NPA	MEP	BO
S1	-0.106	0.171	0.340	-59.167	2.339	-0.101	0.174	0.340	-59.164	2.338
N2	-0.215	-0.583	-0.456	-18.291	3.291	-0.257	-0.586	-0.453	-18.283	3.294
N3	0.370	-0.481	-0.497	-18.250	3.341	0.452	-0.480	-0.483	-18.223	3.383
C8	-0.212	-0.488	-0.708	-14.733	3.816	-0.180	-0.490	-0.711	-14.725	3.811
C11	-0.400	-0.321	-0.477	-14.673	3.756	-0.357	-0.328	-0.474	-14.660	3.745
C12	-0.348	-0.325	-0.481	-14.673	3.759	-0.337	-0.334	-0.479	-14.658	3.748
R(+)-Free base										
GAS						PCM				
Atoms	MK	Mulliken	NPA	MEP	BO	MK	Mulliken	NPA	MEP	BO
S1	-0.344	0.155	0.329	-59.182	2.334	-0.126	0.154	0.327	-59.183	2.332
N2	-0.344	-0.584	-0.455	-18.313	3.303	-0.018	-0.583	-0.454	-18.312	3.304
N3	-0.344	-0.387	-0.511	-18.354	3.112	-0.336	-0.390	-0.504	-18.353	3.104
C8	-0.330	-0.484	-0.695	-14.753	3.836	-0.341	-0.484	-0.694	-14.752	3.837
C11	-0.255	-0.296	-0.472	-14.723	3.815	-0.215	-0.300	-0.476	-14.723	3.816
C12	-0.123	-0.306	-0.469	-14.720	3.821	-0.127	-0.309	-0.473	-14.720	3.822
R(+)-Cationic										
GAS						PCM				
Atoms	MK	Mulliken	NPA	MEP	BO	MK	Mulliken	NPA	MEP	BO
S1	-0.106	0.188	0.349	-59.085	2.343	-0.090	0.190	0.351	-59.088	2.341
N2	0.033	-0.586	-0.471	-18.197	3.263	-0.048	-0.591	-0.460	-18.193	3.276
N3	0.046	-0.495	-0.449	-18.050	3.470	0.033	-0.490	-0.447	-18.047	3.471
C8	-0.145	-0.499	-0.722	-14.597	3.805	-0.155	-0.492	-0.719	-14.593	3.806
C11	-0.308	-0.343	-0.476	-14.521	3.708	-0.298	-0.343	-0.476	-14.519	3.707
C12	-0.384	-0.351	-0.473	-14.519	3.713	-0.358	-0.353	-0.473	-14.517	3.711
R(+)-Hydrochloride										
GAS						PCM				
Atoms	MK	Mulliken	NPA	MEP	BO	MK	Mulliken	NPA	MEP	BO
S1	-0.129	0.158	0.331	-59.173	2.335	-0.122	0.160	0.332	-59.170	2.335
N2	-0.132	-0.588	-0.457	-18.299	3.295	-0.226	-0.588	-0.456	-18.292	3.293
N3	0.407	-0.481	-0.492	-18.244	3.353	0.454	-0.482	-0.479	-18.221	3.389
C8	-0.208	-0.496	-0.710	-14.725	3.818	-0.190	-0.497	-0.712	-14.715	3.816
C11	-0.319	-0.315	-0.476	-14.671	3.753	-0.314	-0.322	-0.475	-14.660	3.743
C12	-0.448	-0.324	-0.472	-14.668	3.760	-0.415	-0.332	-0.471	-14.657	3.749

phase show blue colours on the entire surface but, in particular, strong blue colours it is observed on the protonated N-H region. In the free base species the strong red colours are observed on the N3 atoms and S1 atoms while in the hydrochloride species the strong red colours are observed on the Cl atoms. Hence, the typical nucleophilic sites are clearly identified with red colours while the electrophilic sites with blue colours, as

observed in other species [6, 7, 8, 9].

3.4. NBO study

For the three species of both S(-) and R(+)-PTZ enantiomers the main delocalization energies in gas and aqueous solution were calculated by

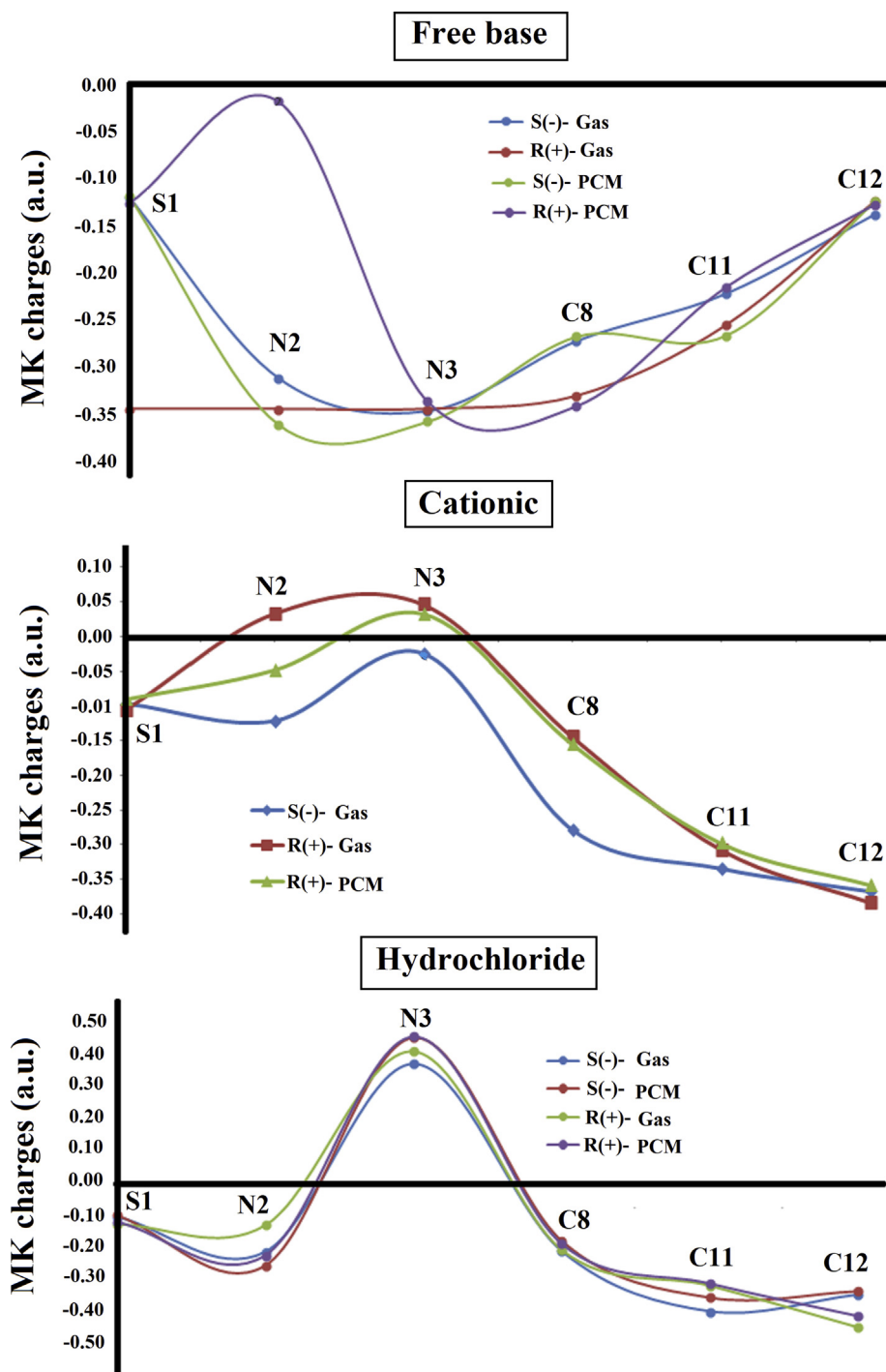


Fig. 4. Calculated Merz-Kollman charges of free base, cationic and hydrochloride species of both S(-) and R(+) enantiomers of promethazine by using the B3LYP/6-31G* method.

using B3LYP/6-31G* calculations with the NBO program [58]. The resulted for the three species of S(-) and R(+)-PTZ are summarized in Tables 7 and 8, respectively. Different interactions can be observed in the three species and, especially in the hydrochloride species due to the presence of Cl atoms where in particular, the $\pi^* \rightarrow \pi^*$ and $\pi \rightarrow \pi^*$ interactions present the higher values in the S(-) and R(+)-PTZ forms, respectively. Thus, the free base (3509.36–3522.22 kJ/mol) and hydrochloride (6253.53–5840.28 kJ/mol) species present higher total energies than the cationic ones (1541.01 kJ/mol) and, for these reasons, these two species are most stable than the cationic ones. However, the

hydrochloride species of R(+)-PTZ have higher values in both media than the corresponding to other enantiomer (7527.88–7332.02 kJ/mol). Nevertheless, the free base of R(+)-PTZ present lower values than the corresponding to S(-)-PTZ (3484.4–3193.04 kJ/mol) while the cationic form of R(+)-PTZ is most stable than the corresponding to S(-)-PTZ (1540.08–1612.71 kJ/mol). These studies shows clearly that the hydrochloride species are most stable than the other two species of both forms and in the two media studied but, in particular the species of R(+)-PTZ show higher total energy values evidencing a slight higher stability than the S(-) one. The three PTZ species show higher stabilities

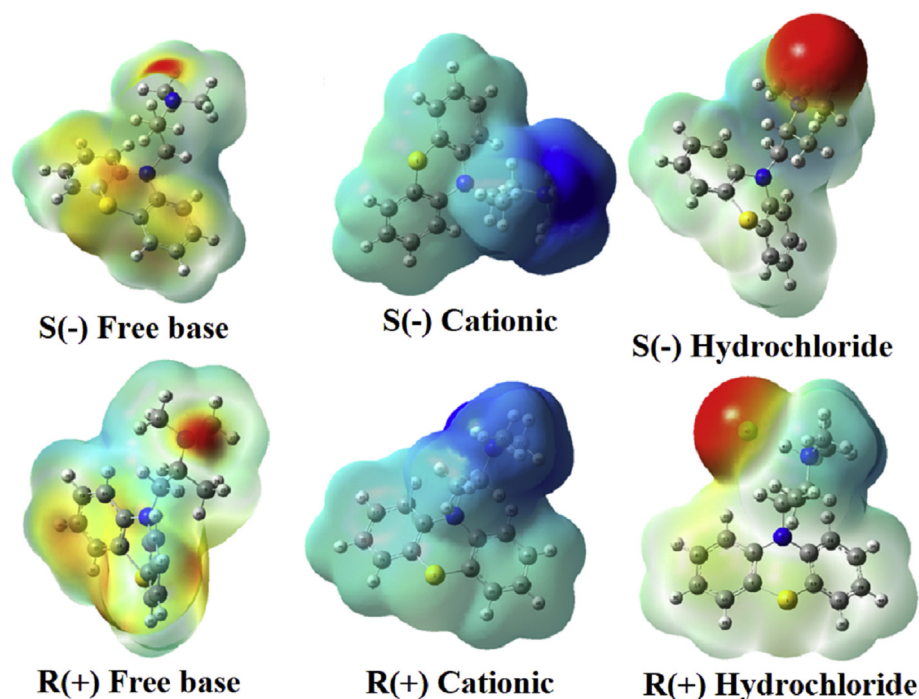


Fig. 5. Calculated electrostatic potential surfaces on the molecular surfaces of the free base, cationic and hydrochloride species of both S(-) and R(+) enantiomers of promethazine. B3LYP functional and 6-31G* basis set. Isodensity value of 0.005.

than the corresponding to cyclizine [9].

3.5. AIM studies

According to the Bader's theory the topological properties are interesting parameters to predict different types of interactions, such as intra or inter-molecular, ionic and hydrogen bonds interactions [59]. Hence, these properties can be easily computed in the bond critical points (BCPs) and in the ring critical points (RCPs) with the AIM2000 program [60]. Here, the electron density, $\rho(r)$, the Laplacian values, $\nabla^2\rho(r)$, the eigenvalues (λ_1 , λ_2 , λ_3) of the Hessian matrix and, the $|\lambda_1|/\lambda_3$ ratio calculated by using the B3LYP/6-31G* method for the three forms of both S(-) and R(+)-PTZ enantiomers can be observed from Tables 9, 10 and 11. Note that the ionic and hydrogen bonds interactions are observed when $\lambda_1/\lambda_3 < 1$ and $\nabla^2\rho(r) > 0$ [9]. Here, RCPN1, RCPN2 and RCPN3 are new RCPs formed as a consequence of C...H and H...H interactions while RCP1, RCP2 and RCP3 are RCPs corresponding to the R1, R2 and R3 rings, as defined in Fig. 1. In all species, the topological properties of RCP1 and RCP3 are practically the same in the two phenyl rings but different from RCP2 because this ring is the phenothiazine ring. First, analyzing the free bases species of both enantiomers, we observed that S(-)-PTZ present two C14...H21 and H...H interactions in both media but the involved atoms change of H24-H32 in gas phase to H23-H33 in solution. In R(+)-PTZ, the free base presents in gas phase the C14...H21 and H22...H31 interactions while in solution are observed three different H...H interactions. In the cationic species of S(-)-PTZ are not observed interactions while in R(+)-PTZ is observed a H...H interaction in gas phase while in solution are observed two C...H and a H...H interactions. The hydrochloride species of S(-)-PTZ present two interactions in gas phase and three different in solution while in the R(+)-PTZ enantiomer in gas phase (Table 11) are observed five interactions and only three in solution. In the hydrochloride species the Cl...H are ionic interactions where in S(-)-PTZ the Cl-H distances are 1.716 Å in gas phase and 2.032 Å in solution while in R(+)-PTZ the distances change to 1.748 Å in gas phase and 2.029 Å in solution. Evidently, both hydrochloride species are the most stable due to the higher values of their topological properties. These results are in agreement with those analyzed by NBO studies. The

hydrochloride species of both forms of PTZ reveals higher stabilities than the corresponding to cyclizine [9].

3.6. Frontier orbitals and global descriptors studies

To predict reactivities and behaviours of both S(-) and R(+)-PTZ forms are of interest to understand why the presence of two N-CH₃ groups in their structures present the same biological activities than cyclizine despite those two groups in PTZ are not linked to rings. Hence, from the frontier orbitals and their differences is possible to compute the gap values [43, 44] and later, by using known equations the chemical potential (μ), electronegativity (χ), global hardness (η), global softness (S), global electrophilicity index (ω) and global nucleophilicity index (E) descriptors can be calculated by using the hybrid B3LYP/6-31G* level of theory [45, 46, 47, 48, 49, 50, 51, 52, 53]. The gap and descriptors values for both PTZ enantiomers in the two media are presented in Table 12. The evaluation of gap values for the three species show easily that the hydrochloride species of both S(-) and R(+)-PTZ forms in solution have low gap values and, for these reasons, the two species are more reactive but the S(-) form is most reactive than the R(+)-PTZ one, as expected because this latter form presents higher stability by NBO analysis ($>$ Total energy). Moreover, the free base and cationic species of S(-) form are most reactive than the corresponding to the R(+) form. Comparisons of these results with the observed for similar species containing N-CH₃ groups, as scopolamine, heroin morphine, cocaine, tropane and cyclizine are presented in Table 13 while their behaviours can be seen in Fig. 6. This figure shows that the hydrochloride species of cocaine in both media present the lower gap values and, obviously, are the most reactive species while in all media the tropane species are the less reactive being, the cationic one in gas phase the less reactive. Note that the free base and cationic species of two forms of PTZ are most reactive than the corresponding to cyclizine, however, the hydrochloride species of cyclizine is most reactive than both forms of PTZ. If now the descriptors are analyzed it is observed from Table 12 that the three species of S(-)-PTZ have higher electrophilicity indexes than the corresponding to R(+) form while, on the contrary, the species of R(+) form have higher nucleophilicity indexes than the species of S(-)-PTZ. The only exception is the

Table 7

Main delocalization energies (in kJ/mol) for three species of S(-)-promethazine in gas and aqueous solution by using B3LYP/6-31G* calculations.

B3LYP/6-31G* ^a	Free base		Hydrochloride	
	Gas	PCM	Gas	PCM
	$\pi C6-C13 \rightarrow \pi^* C9-C15$	74.32	74.28	73.40
$\pi C6-C13 \rightarrow \pi^* C17-C19$	88.41	88.49	85.98	85.77
$\pi C7-C14 \rightarrow \pi^* C10-C16$	74.49	74.61	72.73	72.02
$\pi C7-C14 \rightarrow \pi^* C18-C20$	88.28	88.49	85.23	85.19
$\pi C9-C15 \rightarrow \pi^* C6-C13$	83.56	83.39	85.27	85.27
$\pi C9-C15 \rightarrow \pi^* C17-C19$	71.18	71.27	72.02	71.98
$\pi C10-C16 \rightarrow \pi^* C7-C14$	83.81	83.60	85.90	86.19
$\pi C10-C16 \rightarrow \pi^* C18-C20$	71.52	71.60	72.23	72.10
$\pi C17-C19 \rightarrow \pi^* C6-C13$	79.59	79.59	81.34	81.97
$\pi C17-C19 \rightarrow \pi^* C9-C15$	93.84	93.67	94.09	94.26
$\pi C18-C20 \rightarrow \pi^* C7-C14$	80.05	80.21	82.05	82.26
$\pi C18-C20 \rightarrow \pi^* C10-C16$	93.75	93.67	94.26	94.30
$\Sigma \pi \rightarrow \pi^*$	982.8	982.87	984.5	984.5
$LP(2)S1 \rightarrow \pi^* C9-C15$	45.98	45.44	46.27	46.02
$LP(2)S1 \rightarrow \pi^* C10-C16$	45.98	45.23	46.36	46.27
$LP(1)N2 \rightarrow \pi^* C6-C13$	99.86	99.36	92.96	94.89
$LP(1)N2 \rightarrow \pi^* C7-C14$	100.74	99.44	94.30	97.56
$\Sigma_{LP \rightarrow \pi^*}$	292.56	289.47	279.89	284.74
$\pi^* C9-C15 \rightarrow \pi^* C17-C19$	1106.65	1113.09		
$\pi^* C10-C16 \rightarrow \pi^* C18-C20$	1127.35	1136.79		
$\pi^* C6-C13 \rightarrow \pi^* C17-C19$			1101.14	978.58
$\pi^* C7-C14 \rightarrow \pi^* C18-C20$			909.65	805.44
$\pi^* C9-C15 \rightarrow \pi^* C17-C19$			1057.33	1045.67
$\pi^* C10-C16 \rightarrow \pi^* C18-C20$			1040.23	1046.42
$\Sigma \pi^* \rightarrow \pi^*$	2234	2249.88	4108.35	3876.11
$\sigma N3-C4 \rightarrow LP(1)^*H41$			44.60	62.57
$\sigma N3-C11 \rightarrow LP(1)^*H41$			50.08	62.82
$\sigma N3-C12 \rightarrow LP(1)^*H41$			47.61	60.19
$\Sigma_{\sigma \rightarrow LP^*}$			142.29	185.58
$LP(1)N3 \rightarrow LP(1)^*H41$			1158.49	1456.02
$LP(1)Cl42 \rightarrow LP(1)^*H41$			46.94	16.51
$LP(4)Cl42 \rightarrow LP(1)^*H41$			797.46	306.06
$\Sigma_{LP \rightarrow LP^*}$			2002.89	1778.59
Σ_{TOTAL}	3509.36	3522.22	6253.53	5840.28
Cationic ^a				
Delocalization	Gas			
$\pi C13-C17 \rightarrow \pi^* C6-C9$	47.86			
$\pi C15-C19 \rightarrow \pi^* C6-C9$	43.22			
$\pi C15-C19 \rightarrow \pi^* C13-C17$	46.98			
$\Sigma \pi \rightarrow \pi^*$	138.06			
$\pi C7-C10 \rightarrow LP(1)^*C16$	93.51			
$\pi C18-C20 \rightarrow LP(1)^*C16$	107.22			
$\Sigma \pi \rightarrow LP^*$	200.73			
$LP(1)C14 \rightarrow \pi^* C7-C10$	171.17			
$LP(1)C14 \rightarrow \pi^* C18-C20$	125.57			
$LP(1)C16 \rightarrow \pi^* C7-C10$	176.65			
$LP(1)C16 \rightarrow \pi^* C18-C20$	133.97			
$\Sigma_{LP \rightarrow \pi^*}$	607.36			
$\pi^* C6-C9 \rightarrow \pi^* C13-C17$	361.99			
$\pi^* C6-C9 \rightarrow \pi^* C15-C19$	232.87			
$\Sigma \pi^* \rightarrow \pi^*$	594.86			
Σ_{TOTAL}	1541.01			

The letters bold indicated RMSD values.

^a This work.

hydrochloride species in gas phase of S(-) form because it present a higher value (-7.6061 eV) than the corresponding to R(+) form (7.1020 eV). If both electrophilicity and nucleophilicity indexes of the two S(-) and R(+)-PTZ are compared with other species from Table 14 the behaviours can easily be seen in Fig. 7. Higher electrophilicity indexes are observed in the cationic and hydrochloride species of PTZ than cyclizine while the cationic species of cyclizine have higher nucleophilicity index than both species of PTZ. The higher electrophilicity indexes are observed for all cationic forms in gas phase and, in particular, for cocaine while tropane in both media presents the lowest values. In relation to nucleophilicity indexes, the cationic species of tropane in gas phase presents the highest negative value indicating probably that for these two

Table 8

Main delocalization energies (in kJ/mol) for three species of R(+)-promethazine in gas and aqueous solution by using B3LYP/6-31G* calculations.

B3LYP/6-31G* ^a	Free base		Hydrochloride	
	Gas	PCM	Gas	PCM
	$\pi C6-C13 \rightarrow \pi^* C9-C15$	74.70	74.65	76.53
$\pi C6-C13 \rightarrow \pi^* C17-C19$	88.41	88.49	86.23	85.65
$\pi C7-C14 \rightarrow \pi^* C10-C16$	74.65		72.48	72.23
$\pi C7-C14 \rightarrow \pi^* C18-C20$	88.45		86.82	86.57
$\pi C9-C15 \rightarrow \pi^* C6-C13$	83.43	83.35	83.06	82.51
$\pi C9-C15 \rightarrow \pi^* C17-C19$	71.18	71.14	70.56	70.30
$\pi C10-C16 \rightarrow \pi^* C7-C14$	83.68		84.98	85.77
$\pi C10-C16 \rightarrow \pi^* C18-C20$	71.44		72.15	72.56
$\pi C17-C19 \rightarrow \pi^* C6-C13$	79.80	79.88	82.26	82.93
$\pi C17-C19 \rightarrow \pi^* C9-C15$	93.97	93.97	95.89	96.14
$\pi C18-C20 \rightarrow \pi^* C7-C14$	80.09			80.59
$\pi C18-C20 \rightarrow \pi^* C10-C16$	93.84			93.13
$\Sigma \pi \rightarrow \pi^*$	983.64	491.48	810.96	984.45
$\pi C10-C16 \rightarrow LP(1)^*C7$		202.39		
$\pi C10-C16 \rightarrow LP(1)^*C20$		167.07		
$\pi C14-C18 \rightarrow LP(1)^*C7$		219.66		
$\pi C14-C18 \rightarrow LP(1)^*C20$		183.38		
$\Sigma \pi \rightarrow LP^*$		772.5		
$LP(2)S1 \rightarrow \pi^* C9-C15$	45.73	45.02	44.73	44.77
$LP(2)S1 \rightarrow \pi^* C10-C16$	45.81	45.27	47.23	47.02
$LP(1)N2 \rightarrow \pi^* C6-C13$	99.32	99.44	91.37	92.13
$LP(1)N2 \rightarrow \pi^* C7-C14$	101.03		101.78	100.74
$LP(1)C20 \rightarrow \pi^* C10-C16$		337.28		
$LP(1)C20 \rightarrow \pi^* C14-C18$		305.43		
$\Sigma_{LP \rightarrow \pi^*}$	291.89	832.44	285.11	284.66
$LP(1)^*C7 \rightarrow \pi^* C10-C16$		267.60		
$LP(1)^*C7 \rightarrow \pi^* C14-C18$		258.91		
$\Sigma_{LP^* \rightarrow \pi^*}$				
$\pi^* C9-C15 \rightarrow \pi^* C17-C19$	1084.83			
$\pi^* C10-C16 \rightarrow \pi^* C18-C20$	1123.92			
$\pi^* C6-C13 \rightarrow \pi^* C17-C19$			1247.39	1083.04
$\pi^* C7-C14 \rightarrow \pi^* C18-C20$			1071.67	978.87
$\pi^* C9-C15 \rightarrow \pi^* C17-C19$		1096.62	843.40	817.61
$\pi^* C10-C16 \rightarrow \pi^* C18-C20$			1184.32	1207.85
$\Sigma \pi^* \rightarrow \pi^*$	2208.87	1096.62	4346.78	4087.37
$\sigma N3-C4 \rightarrow LP(1)^*H41$			49.70	61.65
$\sigma N3-C11 \rightarrow LP(1)^*H41$			49.16	59.73
$\sigma N3-C12 \rightarrow LP(1)^*H41$			46.48	57.85
$\Sigma_{\sigma \rightarrow LP^*}$			145.34	179.23
$LP(1)N3 \rightarrow LP(1)^*H41$			1234.86	1491.17
$LP(1)Cl42 \rightarrow LP(1)^*H41$				
$LP(4)Cl42 \rightarrow LP(1)^*H41$			704.83	305.14
$\Sigma_{LP \rightarrow LP^*}$			1939.69	1796.31
Σ_{TOTAL}	3484.4	3193.04	7527.88	7332.02
Cationic ^a				
Delocalization	Gas	PCM		
$\pi C13-C17 \rightarrow \pi^* C6-C9$	47.90	46.98		
$\pi C15-C19 \rightarrow \pi^* C6-C9$	43.30	43.43		
$\pi C15-C19 \rightarrow \pi^* C13-C17$	47.07	47.61		
$\Sigma \pi \rightarrow \pi^*$	138.27	138.02		
$\pi C7-C10 \rightarrow LP(1)^*C16$	93.63	94.47		
$\pi C18-C20 \rightarrow LP(1)^*C16$	107.30	107.05		
$\Sigma \pi \rightarrow LP^*$	200.93	201.52		
$LP(1)N2 \rightarrow \pi^* C6-C9$		42.72		
$LP(1)N2 \rightarrow \pi^* C7-C10$		44.68		
$LP(1)C14 \rightarrow \pi^* C7-C10$	171.67	168.95		
$LP(1)C14 \rightarrow \pi^* C18-C20$	125.57	125.69		
$LP(1)C16 \rightarrow \pi^* C7-C10$	176.65	177.86		
$LP(1)C16 \rightarrow \pi^* C18-C20$	133.72	133.84		
$\Sigma_{LP \rightarrow \pi^*}$	607.61	693.74		
$\pi^* C6-C9 \rightarrow \pi^* C13-C17$	361.78	356.18		
$\pi^* C6-C9 \rightarrow \pi^* C15-C19$	231.49	223.25		
$\Sigma \pi^* \rightarrow \pi^*$	593.27	579.43		
Σ_{TOTAL}	1540.08	1612.71		

The letters bold indicated RMSD values.

^a This work.

Table 9

Analysis of the Bond Critical Points (BCPs) and Ring critical point (RCPs) for three species of S(-)-promethazine in gas and aqueous solution by using the B3LYP/6-31G* method.

B3LYP/6-31G* Method								
Free base								
Gas phase								
Parameter [#]	C14–H21	RCPN1	H24–H32	RCPN2	RCP1	RCP2	RCP3	
$\rho(r)$	0.0088	0.0088	0.0095	0.0095	0.0198	0.0170	0.0198	
$\nabla^2\rho(r)$	0.0333	0.0357	0.0400	0.0421	0.1580	0.1104	0.1580	
λ_1	-0.0043	-0.0036	-0.0084	-0.0080	-0.0146	-0.0055	-0.0145	
λ_2	-0.0011	0.0013	-0.0014	0.0015	0.0815	0.0552	0.0813	
λ_3	0.0388	0.0379	0.0500	0.0485	0.0910	0.0608	0.0911	
$ \lambda_1 /\lambda_3$	0.1108	0.0950	0.1680	0.1649	0.1604	0.0905	0.1592	
Distances (Å)	2.693		2.190					
Aqueous solution								
Parameter [#]	C14–H21	RCPN1	H23–H33	RCPN2	RCP1	RCP2	RCP3	
$\rho(r)$	0.0093	0.0090	0.0133	0.0133	0.0198	0.0169	0.0198	
$\nabla^2\rho(r)$	0.0344	0.0398	0.0626	0.0656	0.1573	0.1103	0.1572	
λ_1	-0.0049	-0.0026	-0.0084	-0.0077	-0.0145	-0.0055	-0.0144	
λ_2	0.0035	0.0050	-0.0019	0.0020	0.0809	0.0569	0.0808	
λ_3	0.0429	0.0375	0.0729	0.0712	0.0909	0.0590	0.0908	
$ \lambda_1 /\lambda_3$	0.1142	0.0693	0.1152	0.1081	0.1595	0.0932	0.1586	
Distances (Å)	2.646		2.086					
Cationic								
Gas phase								
Parameter [#]	RCP1	RCP2	RCP3					
$\rho(r)$	0.0199	0.0173	0.0199					
$\nabla^2\rho(r)$	0.1584	0.1084	0.1586					
λ_1	-0.0146	-0.0050	-0.0146					
λ_2	0.0832	0.0469	0.0835					
λ_3	0.0896	0.0665	0.0896					
$ \lambda_1 /\lambda_3$	0.1629	0.0752	0.1629					
Hydrochloride								
Gas phase								
Parameter [#]	Cl42–H25		Cl42–H41	RCPN1	RCP1	RCP2	RCP3	
$\rho(r)$	0.0080		0.0804	0.0080	0.0198	0.0171	0.0198	
$\nabla^2\rho(r)$	0.0263		0.0866	0.0284	0.1582	0.1100	0.1582	
λ_1	-0.0062		-0.1359	-0.0062	-0.0146	-0.0053	-0.0145	
λ_2	-0.0017		-0.1357	0.0018	0.0822	0.0530	0.0820	
λ_3	0.0342		0.3583	0.0327	0.0905	0.0624	0.0906	
$ \lambda_1 /\lambda_3$	0.1813		0.3793	0.1896	0.1613	0.0849	0.1600	
Distances (Å)	2.908		1.716					
Aqueous solution								
Parameter [#]	C13–H23	RCPN1	H22–28	RCPN2	Cl42–H41	RCP1	RCP2	RCP3
$\rho(r)$	0.0134	0.0133	0.0090	0.0090	0.0416	0.0198	0.0169	0.0198
$\nabla^2\rho(r)$	0.0617	0.0666	0.0384	0.0398	0.0764	0.1574	0.1094	0.1574
λ_1	-0.0093	-0.0081	-0.0079	-0.0074	-0.0534	-0.0145	-0.0056	-0.0145
λ_2	-0.0031	0.0036	-0.0014	0.0014	-0.0532	0.0813	0.0552	0.0811
λ_3	0.0742	0.0711	0.0476	0.0458	0.1828	0.0906	0.0597	0.0907
$ \lambda_1 /\lambda_3$	0.1253	0.1139	0.1660	0.1616	0.2921	0.1600	0.0938	0.1599
Distances (Å)	2.508		2.189		2.032			

[#] This symbol implies values in a.u. units.

reasons, this species is the less reactive than the other ones (see Table 13).

3.7. Vibrational study

B3LYP calculations have optimized the three species of S(-) and R(+)-PTZ forms with C_1 symmetries. The normal vibration modes expected for the free base, cationic and hydrochloride species are respectively 114, 117 and 120 and, where all modes are active, in both spectra. The experimental available infrared and Raman spectra for promethazine hydrochloride were taken from Refs [10] and [66]. The experimental IR

from Ref [66] was compared with the corresponding predicted for the three species of both enantiomers in Fig. 8 while the comparisons of the corresponding predicted Raman spectra with the experimental one are given in Fig. 9. Evidently, the hydrochloride forms of both enantiomers are not present in the experimental IR spectrum because the predicted intense IR bands of both S(-) and R(+) forms at 1625 and 1713 cm^{-1} respectively are not observed in the experimental one with the same intensities. Besides, the predicted IR spectra in the 2000–500 cm^{-1} region show strong differences between the intensities of IR bands at 1459 and 759 cm^{-1} in the three species of both S(-) and R(+)-PTZ enantiomers but when only the average of cationic forms by using frequencies and

Table 10

Analysis of the Bond Critical Points (BCPs) and Ring critical point (RCPs) for free base and cationic species of R(+)-promethazine in gas and aqueous solution by using the B3LYP/6-31G* method.

B3LYP/6-31G* Method									
Free base									
Gas phase									
Parameter [#]	C14–H21	RCPN1	H22–H31	RCPN2	RCP1	RCP2	RCP3		
$\rho(r)$	0.0084	0.0084	0.0120	0.0110	0.0198	0.0170	0.0198		
$\nabla^2\rho(r)$	0.0315	0.0332	0.0483	0.0571	0.1580	0.1105	0.1580		
λ_1	-0.0037	-0.0033	-0.0127	0.0078	-0.0146	-0.0055	-0.0145		
λ_2	-0.0008	0.0009	-0.0083	0.0107	0.0815	0.0551	0.0813		
λ_3	0.0362	0.0355	0.0694	0.0542	0.0911	0.0609	0.0911		
$ \lambda_1 /\lambda_3$	0.1022	0.0930	0.1830	-0.1439	0.1603	0.0903	0.1592		
Distances (Å)	2.727		2.024						
Aqueous solution									
Parameter [#]	H31–H34	H22–H31	RCPN1	H23–H33	RCPN2	RCP1	RCP2	RCP3	
$\rho(r)$	0.0057	0.0128	0.0057	0.0132	0.0132	0.0198	0.0170	0.0198	
$\nabla^2\rho(r)$	0.0212	0.0511	0.0208	0.0605	0.0656	0.1573	0.1103	0.1572	
λ_1	-0.0041	-0.0137	-0.0038	-0.0093	-0.0080	-0.0145	-0.0055	-0.0144	
λ_2	-0.0022	-0.0092	0.0029	-0.0033	0.0039	0.0809	0.0559	0.0807	
λ_3	0.0275	0.0742	0.0216	0.0732	0.0697	0.0909	0.0598	0.0909	
$ \lambda_1 /\lambda_3$	0.1491	0.1846	0.1759	0.1270	0.1148	0.1595	0.0920	0.1584	
Distances (Å)	2.353	1.995		2.072					
Cationic									
Gas phase									
Parameter [#]	H22–H31	RCPN1	RCP1	RCP2	RCP3				
$\rho(r)$	0.0120	0.0108	0.0199	0.0173	0.0199				
$\nabla^2\rho(r)$	0.0478	0.0533	0.1584	0.1084	0.1588				
λ_1	-0.0131	-0.0087	-0.0146	-0.0049	-0.0146				
λ_2	-0.0086	0.0107	0.0832	0.0472	0.0836				
λ_3	0.0696	0.0513	0.0897	0.0664	0.0896				
$ \lambda_1 /\lambda_3$	0.1882	0.1696	0.1628	0.0738	0.1629				
Distances (Å)	2.008								
Aqueous solution									
Parameter [#]	C14–H21	RCPN1	C13–H23	RCPN2	H22–H31	RCPN3	RCP1	RCP2	RCP3
$\rho(r)$	0.0085	0.0085	0.0131	0.0131	0.0124	0.0112	0.0198	0.0169	0.0198
$\nabla^2\rho(r)$	0.0326	0.03369	0.0617	0.0639	0.0495	0.0556	0.1576	0.1095	0.1575
λ_1	-0.0033	-0.0030	-0.0085	-0.0080	-0.0135	-0.0090	-0.0145	-0.0056	-0.0145
λ_2	-0.0006	0.0006	-0.0014	0.0015	-0.0087	0.0108	0.0815	0.0553	0.0811
λ_3	0.0366	0.0360	0.0716	0.0704	0.0717	0.0538	0.0906	0.0598	0.0908
$ \lambda_1 /\lambda_3$	0.0902	0.0833	0.1187	0.1136	0.1883	0.1673	0.1600	0.0936	0.1597
Distances (Å)	2.718		2.520		1.996				

[#] This symbol implies values in a.u. units.

Table 11

Analysis of the Bond Critical Points (BCPs) and Ring critical point (RCPs) for three species of R(+)-promethazine in gas and aqueous solution by using the B3LYP/6-31G* method.

B3LYP/6-31G* Method												
Hydrochloride												
Gas phase												
Parameter [#]	C5...H34	RCPN1	C13...H23	RCPN2	H22...H31	RCPN3	C142...H23	C142...H41	RCPN3	RCP1	RCP2	RCP3
$\rho(r)$	0.0112	0.0112	0.0130	0.0130	0.0120	0.0109	0.0093	0.0746	0.0082	0.0198	0.0170	0.0199
$\nabla^2\rho(r)$	0.0508	0.0508	0.0624	0.0624	0.0484	0.0548	0.0311	0.0935	0.0343	0.1580	0.1096	0.1584
λ_1	-0.0092	-0.0092	-0.0090	-0.0090	-0.0130	-0.0087	-0.0072	-0.1220	-0.0057	-0.0146	-0.0055	-0.0146
λ_2	-0.0005	-0.0005	-0.0006	-0.0006	-0.0085	0.0107	-0.0051	-0.1219	0.0068	0.0815	0.0535	0.0820
λ_3	0.0606	0.0606	0.0720	0.0720	0.0699	0.0528	0.0435	0.3374	0.0331	0.0910	0.0615	0.0909
$ \lambda_1 /\lambda_3$	0.1518	0.1518	0.1250	0.1250	0.1860	0.1648	0.1655	0.3616	0.1722	0.1604	0.0894	0.1606
Distances (Å)	2.637		2.520		2.008		2.814	1.748				
Aqueous solution												
Parameter [#]	C13...H23	RCPN1	H22...H31	RCPN2	C142...H41	RCP1	RCP2	RCP3				
$\rho(r)$	0.0134	0.0134	0.0122	0.0111	0.0418	0.0198	0.0169	0.0198				
$\nabla^2\rho(r)$	0.0633	0.0668	0.0494	0.0558	0.0771	0.1575	0.1093	0.1576				
λ_1	-0.0094	-0.0085	-0.0131	-0.0088	-0.0536	-0.0145	-0.0057	-0.0145				
λ_2	-0.0023	0.0025	-0.0085	0.0106	-0.0535	0.0813	0.0557	0.0808				
λ_3	0.0750	0.0726	0.0711	0.0537	0.1843	0.0907	0.0592	0.0911				
$ \lambda_1 /\lambda_3$	0.1253	0.1171	0.1842	0.1639	0.2908	0.1599	0.0963	0.1592				
Distances (Å)	2.507		1.999		2.029							

[#] This symbol implies values in a.u. units.

Table 12

Frontier molecular HOMO and LUMO orbitals, gap values and descriptors for the three species of S(-) and R(+)-promethazine (in eV) in gas and aqueous solution by using the B3LYP/6-31G* level of theory.

Orbitals	Free base		Cationic		Hydrochloride	
	Gas	PCM	Gas	PCM	Gas	PCM
S(-)-promethazine						
HOMO	-5.0096	-5.0559	-7.943		-5.5593	-5.0151
LUMO	-0.2939	-0.2857	-3.3769		-0.6939	-0.8109
GAP	4.7157	4.7702	4.5661		4.8654	4.2042
Descriptors						
χ	-2.3579	-2.3851	-2.2831		-2.4327	-2.1021
μ	-2.6518	-2.6708	-5.6600		-3.1266	-2.9130
η	2.3579	2.3851	2.2831		2.4327	2.1021
S	0.2121	0.2096	0.2190		0.2055	0.2379
ω	1.4911	1.4954	7.0158		2.0092	2.0184
E	-6.2524	-6.3701	-12.9219		-7.6061	-6.1234
R(+)-promethazine						
HOMO	-5.0504	-5.0776	-7.9403	-5.5593	-5.3579	-5.1538
LUMO	-0.2748	-0.2748	-3.3633	-0.6939	-0.5469	-0.6612
GAP	4.7756	4.8028	4.5770	4.8654	4.8110	4.4926
Descriptors						
χ	-2.3878	-2.4014	-2.2885	-2.4327	-2.4055	-2.2463
μ	-2.6626	-2.6762	-5.6518	-3.1266	-2.9524	-2.9075
η	2.3878	2.4014	2.2885	2.4327	2.4055	2.2463
S	0.2094	0.2082	0.2185	0.2055	0.2079	0.2226
ω	1.4845	1.4912	6.9790	2.0092	1.8118	1.8817
E	-6.3578	-6.4266	-12.9341	-7.6061	-7.1020	-6.5311

$\chi = -[E(\text{LUMO}) - E(\text{HOMO})]/2$; $\mu = [E(\text{LUMO}) + E(\text{HOMO})]/2$; $\eta = [E(\text{LUMO}) - E(\text{HOMO})]/2$.

$S = 1/2\eta$; $\omega = \mu^2/2\eta$; $E = \mu*\eta$.

intensities Lorentzian band shapes for a 1:1 population ratio of each species the ratio between those two bands decreases notably, as shown in Fig. 10. Note that in the higher wavenumbers region the predicted IR spectra for both cationic species are similar to the corresponding

Table 13

Frontier molecular HOMO and LUMO orbitals and gap values for the three species of S(-) and R(+)-promethazine compared with other species in gas and aqueous solution phases by using the B3LYP/6-31G* level of theory.

Orbital	Scopolamine ^{a,b}	Heroin ^c	Morphine ^d	Cocaine ^e	Tropane ^f	Cyclizine ^g	Promethazine ^a	
							S(-)	R(+)
Free base/Gas phase								
GAP	5.4004	5.6563	5.6044	4.8580	7.5506	5.3946	4.7157	4.7756
Free base/Aqueous solution								
GAP	5.4758	5.6414	5.4750	4.9487	7.6611	5.5067	4.7702	4.8028
Cationic/Gas phase								
GAP	5.6356	5.4268	5.1889	5.4468	9.5595	5.5823	4.5661	4.5770
Hydrochloride/Gas phase								
GAP	4.9239	5.3024	5.4417	3.6813	6.8246		4.8654	4.8110
Hydrochloride/Aqueous solution								
GAP	5.4026	4.4469	4.5840	3.6813	5.9119	4.2159	4.2042	4.4926

[#] Hydrobromide.

^a This work.

^b From Ref [7].

^c From Ref [5].

^d From Ref [1].

^e From Ref [3].

^f From Ref [2].

^g From Ref [9].

experimental ones. Hence, it is evident the presence of both cationic species of S(-) and R(+)-PTZ in the solid phase, as revealed by Borodi et al [19]. The normal internal coordinates, the SQMFF methodology [39] and the Molvib program [42] were used to calculate the harmonic force fields in order to perform the complete vibrational assignments of all species of DHC. The scale factors used were those reported in the literature [40]. In Table 15 are presented the experimental and calculated wavenumbers together with the assignments of three species of S(-) and R(+)-PTZ forms, respectively. Below, discussions of assignments for some groups are presented.

3.7.1. Band assignments

3.7.1.1. N-H modes. For both PTZ forms, the NH stretching modes are expected only for the cationic and hydrochloride species. For instance, in monomer and dimer of clonidine hydrochloride [67] these modes are assigned at 3427/3341 and 2584 cm⁻¹, respectively while in those two forms of diphenhydramine [8] these modes are predicted respectively at 3150 and 1748 cm⁻¹. Here, in the cationic and hydrochloride species of S(-) form of DHC these modes are predicted to 3295 and 1638 cm⁻¹ and in the R(+) form they are predicted to 3273 and 1713 cm⁻¹. Then, they can be assigned in the same region. Here, the group of bands observed in IR spectrum of DHC between 2800 and 2200 cm⁻¹ with a strong band centered at 2370 cm⁻¹ could be assigned to the N-H stretching modes due to H bonds, as was also reported for clonidine hydrochloride [67]. The N-H rocking modes for both cationic and hydrochloride forms are predicted in different regions, as observed in Table 15. Later, these modes are assigned in accordance. The torsion $\tau_{\text{N3-H41}}$ modes expected only in both hydrochloride forms are predicted by calculations to 105 and 70 cm⁻¹ and they cannot be assigned because there are not observed bands in this region.

3.7.1.2. CH modes. In the three species of both S(-) and R(+)-PTZ enantiomers, eight aromatics C-H stretching modes are expected and only one stretching mode (C4-H21) with aliphatic characteristic. Hence, they are predicted by the SQM/B3LYP/6-31G* calculations in different regions. Evidently, the aromatics modes are assigned at higher

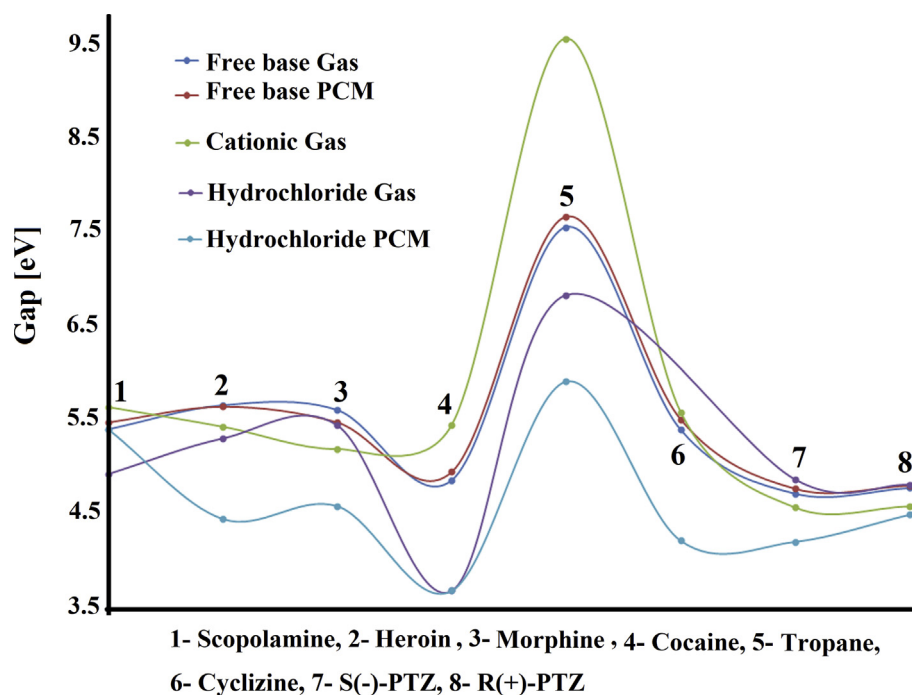


Fig. 6. Calculated gap values of free base, cationic and hydrochloride species of both S(-) and R(+) enantiomers of promethazine in both media by using the B3LYP/6-31G* method compared with reported values for alkaloids and antihistaminic agents.

wavenumbers than the other ones, as shown in Tables 15 and 16. Besides, the in-plane deformation or rocking and out-of-plane deformation modes expected only for these C-H aromatics are predicted respectively between 1489/1120 and 987/745 cm^{-1} . Hence, they can be assigned in these regions. These modes in carquejol [50] are assigned between

1483/1121 and 972/746 cm^{-1} .

3.7.1.3. *CH₃ modes.* The three species of both S(-) and R(+)-PTZ enantiomers present three CH₃ groups, where two of them are linked to N3 atoms and the other one to C4 atoms. Then, these modes are predicted in

Table 14

Global electrophilicity (ω) and nucleophilicity (E) indexes for the three species of S(-) and R(+)-promethazine compared with other species in gas and aqueous solution phases by using the B3LYP/6-31G* level of theory.

Descriptor	Scopolamine ^{#,b}	Heroin ^c	Morphine ^d	Cocaine ^e	Tropane ^f	Cyclizine ^g	Promethazine ^a	
							S(-)	R(+)
Free base/Gas phase ^a								
ω	1.7393	1.5083	1.3639	2.5183	0.3914	1.6777	1.4911	1.4845
E	-8.2756	-8.2606	-7.7475	-8.4959	-6.4905	-8.1146	-6.2524	-6.3578
Free base/Aqueous solution ^a								
ω	1.7504	1.5180	1.2339	2.5297	0.4429	1.7288	1.4954	1.4912
E	-8.4763	-8.2545	-7.1153	-8.7546	-7.0557	-8.4953	-6.3701	-6.4266
Cationic/gas phase ^a								
ω	6.4529	6.7459	6.8155	7.9799	6.9598	6.5083	7.0158	6.9790
E	-16.9925	-16.4174	-15.4288	-17.9548	-38.9872	-16.8238	-12.9219	-12.9341
Hydrochloride/Aqueous solution ^a								
ω	0.9799	1.9667	1.8414	2.6828	0.6421	1.9053	2.0184	1.8817
E	-6.2154	-6.5755	-6.6589	-5.7845	-5.7592	-5.9742	-6.1234	-6.5311

$\omega = \mu^2/2\eta$; $E = \mu^*\eta$.

Hydrobromide.

^a This work.

^b From Ref [7].

^c From Ref [5].

^d From Ref [1].

^e From Ref [3].

^f From Ref [2].

^g From Ref [9].

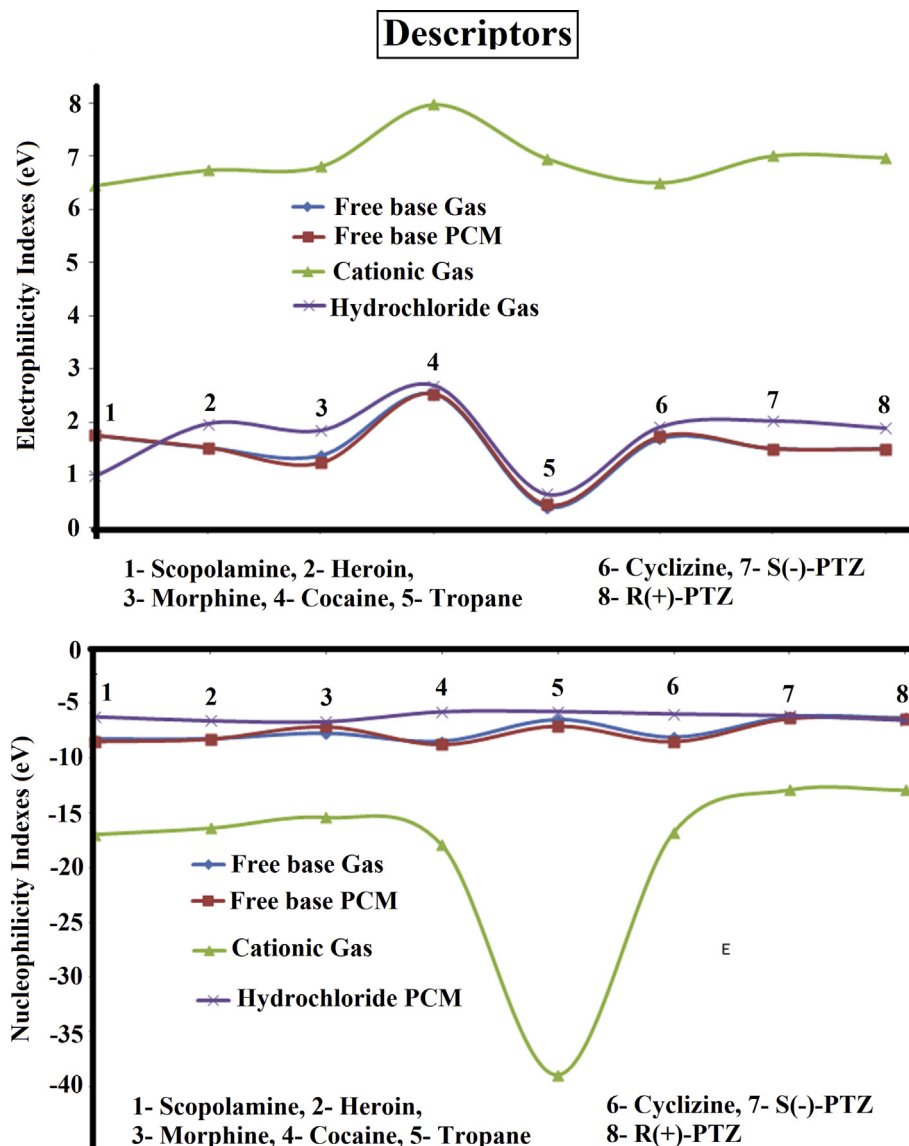


Fig. 7. Calculated electrophilicity indexes of free base, cationic and hydrochloride species of both S(-) and R(+) enantiomers of promethazine in both media by using the B3LYP/6-31G* method.

different regions and, thus, they can be easily assigned in accordance to the calculations. In carquejol [50] these stretching modes are assigned between 3031 and 2919 cm^{-1} while in this case these modes are assigned to the IR and Raman bands between 3411 and 2747 cm^{-1} . Note that the symmetrical stretching modes corresponding to CH_3 groups linked to N3 atoms of two free base species of both S(-) and R(+)-PTZ are predicted at lower wavenumbers and, hence, they are assigned to the IR bands at 2824 and 2747 cm^{-1} . The CH_3 deformation, rocking and twisting modes in carquejol [50] are respectively assigned between 1587/1436, 1084/1026 and 220/171 cm^{-1} . Here, those three vibration modes are assigned to the IR and Raman bands to 1500/1340, 1289/902 and 267/154 cm^{-1} . These latter modes between 178 and 154 couldn't be assigned due to that there are not observed bands in these regions.

3.7.1.4. CH_2 modes. All PTZ species have only one CH_2 group, for which, the expected antisymmetrical and symmetrical stretching,

deformation, wagging, rocking and twisting modes are clearly assigned as predicted by the calculations. For the free base and hydrochloride species of R(+)-PTZ the antisymmetrical modes are predicted at higher wavenumbers than the other species of S(-) form, hence, those modes are assigned to the groups of IR and Raman bands at 3037/2872, 1470/1433, 1421/1387, 1354/1247 and 817/808 cm^{-1} . Those vibration modes of the two CH_2 groups of Carquejol are assigned in approximately the same regions [50].

3.7.1.5. Skeletal modes. In the three species of both S(-) and R(+)-PTZ enantiomers are very important the N3-C11 and N3-C12 stretching modes because their corresponding bonds are predicted by B3LYP/6-31G* calculations longer than the corresponding to N3-C4 bonds, as was experimentally observed by X-ray diffraction [19]. Therefore, the strong IR bands at 1012, 987, 955 and 893 cm^{-1} could be associated to the N3-C11 and N3-C12 stretching modes. Note that the IR band of

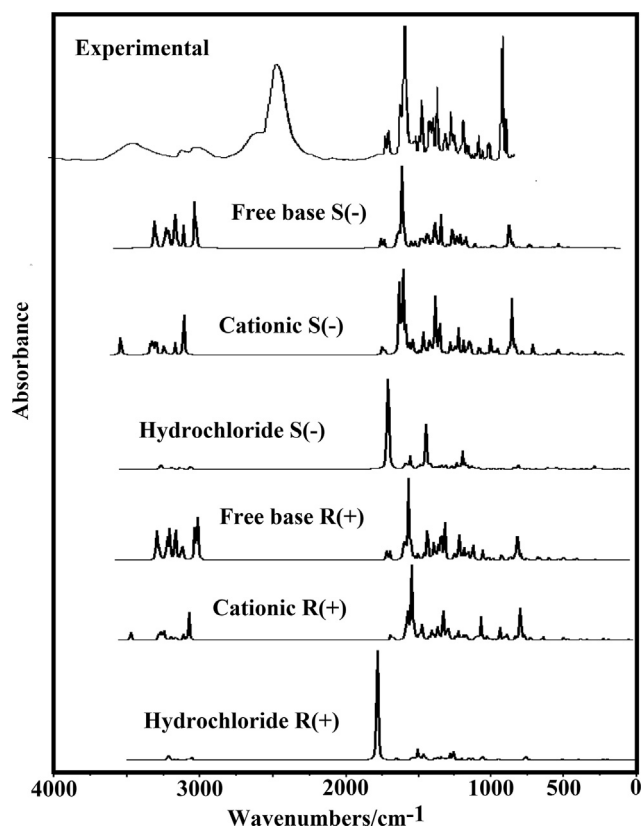


Fig. 8. Experimental infrared spectrum of hydrochloride promethazine compared with the corresponding predicted for the free base, cationic and hydrochloride species of both S(-) and R(+) enantiomers by using B3LYP/6-31G* level of theory.

medium intensity at 1256 cm^{-1} could be also attributed to the N3–C4 stretching mode of free base of S(-)-PTZ while the strong IR band at 1189 cm^{-1} could be assigned to the N3–C11 stretching mode of free base of that form. Moreover, the very strong IR band at 759 cm^{-1} and the band at 893 cm^{-1} could be associated to N3–C4 stretching modes of both forms. The IR bands at 1128 , 1208 and 1105 cm^{-1} could be assigned to other N–C stretching modes (N2–C5, N2–C6 and N2–C7) expected for all species of PTZ because the calculations predicted these modes in those regions. The C=C stretching modes are usually assigned between 1680 and 1659 cm^{-1} [1-3,5-9,45,47-50,52,53,67]; thus, the strong IR bands at 1558 cm^{-1} is without difficulty associated to these vibration modes of three species of both enantiomeric forms. Here, a very important result is the very strong Raman band observed at 1027 cm^{-1} which is attributed to C–C stretching modes of both phenyl rings of both forms, as was reported for identification of PTZ by Assi [22]. In the IR spectrum that band is observed with medium intensity at 1034 cm^{-1} . The two C9–S1 and C10–S1 stretching modes expected in all species of both enantiomers can be associated to the IR band of medium intensity at 423 cm^{-1} because all species, with exception of free base of S(-) form, are predicted in this region. In the free base of S(-) form the C9–S1 stretching mode is predicted at 1080 cm^{-1} coupled with the N2–C5 stretching mode. The remaining skeletal modes including the deformation and torsion modes of both phenyl rings are assigned in the regions predicted by SQM calculations and according the assignments for similar compounds [1, 2, 3, 5, 6, 7, 8, 9, 45, 47, 48, 49, 50, 52, 53, 67], as detailed in Table 15.

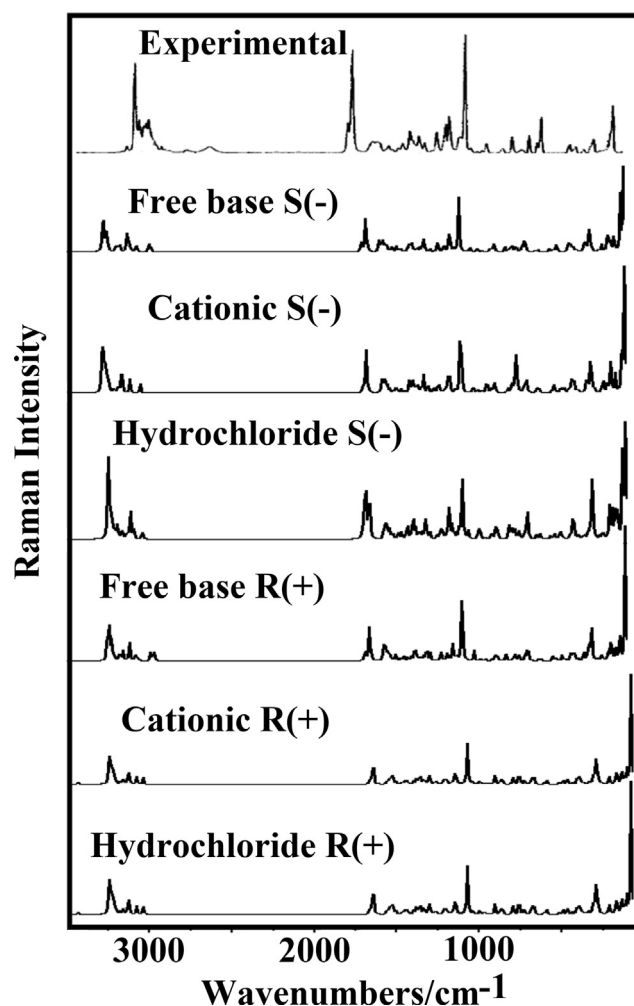


Fig. 9. Experimental Raman spectrum of hydrochloride promethazine compared with the corresponding predicted for the free base, cationic and hydrochloride species of both S(-) and R(+) enantiomers by using B3LYP/6-31G* level of theory.

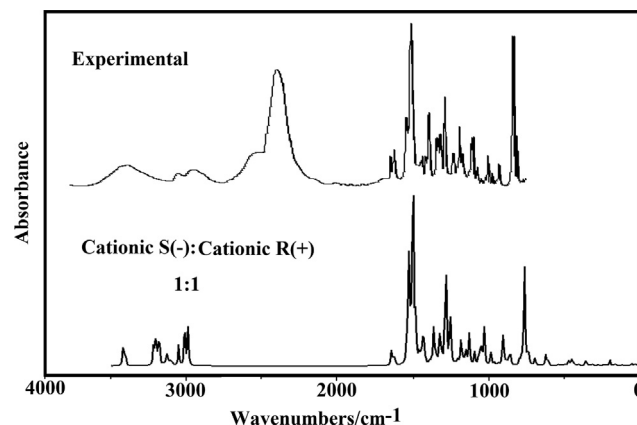


Fig. 10. Experimental infrared spectrum of hydrochloride promethazine compared with the corresponding average predicted for the cationic species of both S(-) and R(+) enantiomers by using frequencies and intensities Lorentzian band shapes for a 1:1 population ratio of each species at B3LYP/6-31G* level of theory.

Table 15 (continued)

Experimental			B3LYP/6-31G* Method ^a											
			S(-)-PTZ						R(+)-PTZ					
			Free base		Cationic		Hydrochloride		Free base		Cationic		Hydrochloride	
IR ^c	IR ^d	Raman ^e	SQM ^b	Assignments ^a	SQM ^b	Assignments ^a	SQM ^b	Assignments ^a	SQM ^b	Assignments ^a	SQM ^b	Assignments ^a	SQM ^b	Assignments ^a
		1558s	1556	ν C13-C17	1558	ν C7-C14	1557	ν C13-C17						
	1550w	1552sh	1550	ν C17-C19 ν C18-C20	1554	ν C17-C19	1552	ν C17-C19 ν C18-C20					1498	ρ N3-H41
1489m	1500w								1489	β C13-H33 β C16-H36	1486	δ_a CH ₃ (C8)	1488	β C14-H34
1466sh	1480sh	1470w					1473	ρ N3-H41	1483	δ_a CH ₃ (C8)	1484	δ_a CH ₃ (C8)	1480	δ_a CH ₃ (C8)
1466sh		1470w							1474	δ CH ₂	1478	δ_a CH ₃ (C12)	1476	δ CH ₂
1466sh		1470w					1470	β C16-H36 β C14-H34	1471	δ_a CH ₃ (C11) δ_a CH ₃ (C12)			1473	δ_a CH ₃ (C8)
1466sh		1470w	1469	β C16-H36 β C14-H34 β C13-H33	1467	β C15-H35 β C13-H33 β C14-H34			1468	δ_a CH ₃ (C8)	1468	δ_a CH ₃ (C8)		
1459vs	1454sh								1463	δ_a CH ₃ (C12)	1463	δ_a CH ₃ (C11)	1464	δ_a CH ₃ (C11) δ_a CH ₃ (C12)
1459vs	1454sh		1456	δ_a CH ₃ (C12) δ_a CH ₃ (C11)	1456	δ_a CH ₃ (C11)			1458	δ_a CH ₃ (C11)	1460	β C14-H34 β C13-H33	1461	δ_a CH ₃ (C12)
1459vs	1454sh				1452	δ_a CH ₃ (C11)	1454	δ CH ₂	1455	δ CH ₂	1453	δ CH ₂	1454	δ CH ₂
	1451sh		1451	δ CH ₂	1451	δ_a CH ₃ (C12)	1451	δ_a CH ₃ (C8)	1450	δ_a CH ₃ (C12)	1451	δ_a CH ₃ (C11)	1449	δ_a CH ₃ (C11)
1447sh	1447sh		1444	δ_a CH ₃ (C8)	1446	δ_a CH ₃ (C8) δ_a CH ₃ (C12)	1449	δ_a CH ₃ (C11)			1447	β C20-H40 β C18-H38	1447	β C20-H40 β C18-H38
1447sh	1447sh		1440	δ_a CH ₃ (C8)	1444	δ_a CH ₃ (C12)	1442	β C13-H33	1446	β C20-H40 β C18-H38	1446	β C19-H39	1446	β C19-H39
1433sh	1438sh		1437	δ_a CH ₃ (C12) δ_a CH ₃ (C8)	1440	δ CH ₂	1438	δ_a CH ₃ (C8)	1444	β C19-H39	1442	δ_a CH ₃ (C12)	1443	δ_a CH ₃ (C11) δ_a CH ₃ (C12)
1433sh	1438sh	1435sh	1435	δ_a CH ₃ (C8)	1432	β C19-H39	1438	δ_a CH ₃ (C12)						
			1430	δ_a CH ₃ (C12)	1431	β C20-H40 β C17-H37	1430	β C20-H40	1435	δ_s CH ₃ (C12) δ_s CH ₃ (C11)				
			1429	β C17-H37 β C19-H39	1429	δ_a CH ₃ (C11) δ_s CH ₃ (C12)	1429	β C19-H39			1427	δ_s CH ₃ (C12)	1425	wagCH ₂ ρ' N3-H41
			1427	β C19-H39	1423	δ_a CH ₃ (C8)	1426	δ_a CH ₃ (C12)	1406	wagCH ₂	1407	wagCH ₂	1420	wagCH ₂
	1419sh		1417	δ_a CH ₃ (C11)	1411	δ_a CH ₃ (C12)	1420	δ_a CH ₃ (C11)			1400	ρ N3-H41	1408	δ_s CH ₃ (C11)
1408vv	1403sh		1406	δ_s CH ₃ (C11)	1400	δ_a CH ₃ (C8)	1408	ρ' N3-H41	1402	wagCH ₂ δ_s CH ₃ (C11)	1397	δ_s CH ₃ (C11)	1401	δ_s CH ₃ (C12)
1390vv	1395sh				1392	ρ' N3-H41 wagCH ₂	1394	wagCH ₂			1394	ρ' N3-H41		
1378w		1387w	1388	wagCH ₂	1381	ρ N3-H41	1376	δ_s CH ₃ (C11) δ_s CH ₃ (C12)	1375	δ_s CH ₃ (C8) ρ' C4-H21	1380	δ_s CH ₃ (C8)	1379	δ_s CH ₃ (C8)
	1364sh	1374vw	1376	δ_s CH ₃ (C12)	1379	δ_s CH ₃ (C11)	1360	δ_s CH ₃ (C8)						
1354w			1362	ρ C4-H21	1361	δ_a CH ₃ (C8)	1355	ν N3-H41 δ_a CH ₃ (C12)	1357	δ_s CH ₃ (C8)	1350	ρ' C4-H21 ρ CH ₂	1356	ρ' C4-H21
1342sh	1347sh	1340w	1342	δ_s CH ₃ (C8)	1349	ρ C4-H21	1351	ρ C4-H21						
1334m	1327sh	1326sh	1323	ρ' C4-H21					1335	ρ' C4-H21	1330	ρ C4-H21 ν N2-C6	1327	ρ CH ₂ ν N2-C6
		1320w			1319	ρ CH ₂ ν N2-C6	1320	ρ' C4-H21	1318	ρ C4-H21	1320	ρ' C4-H21	1313	ρ C4-H21
1292sh	1312sh	1315sh	1309	ν N2-C6 ρ CH ₂	1307	ρ' C4-H21	1315	ν N2-C6	1301	ν C6-C13	1300	ν C6-C13	1301	ν C6-C13
1285m	1294s	1296sh							1286	β C15-H35 ν C16-C10	1282	ν C9-C15 ν C6-C9 ν C7-C10	1288	β C15-H35 β C13-H33
1285m	1294s	1296sh	1283	ν C6-C13	1282	ν C6-C13	1283	ν C6-C13	1285	ν C9-C15 ν C6-C9	1286	β C15-H35	1285	ν C16-C10 ν C7-C10 ν C6-C9

Table 15 (continued)

Experimental			B3LYP/6-31G* Method ^a											
			S(-)-PTZ						R(+)-PTZ					
			Free base		Cationic		Hydrochloride		Free base		Cationic		Hydrochloride	
IR ^c	IR ^d	Raman ^e	SQM ^b	Assignments ^a	SQM ^b	Assignments ^a	SQM ^b	Assignments ^a	SQM ^b	Assignments ^a	SQM ^b	Assignments ^a	SQM ^b	Assignments ^a
1270m	1279sh	1289m	1273	β C15-H35 ν C16-C10	1274	ν C16-C10 ν C9-C15	1275	ν C16-C10	1270	ν N3-C4 ρ CH ₃ (C12)				
		1274sh	1267	ν C9-C15 ν C6-C9 ν C7-C10										
1256m		1253sh	1265	ν N3-C4	1264	ν C7-C10 ν C6-C9	1266	ν C9-C15 ν C7-C10 ν C6-C9	1267	ρ CH ₂	1266	ρ CH ₂	1269	ρ CH ₂ β C16-H36
1249sh		1247m	1253	ρ CH ₂	1255	ρ CH ₂ β C16-H36	1260	ρ CH ₂						
1228m	1233sh	1236sh			1233	ν N2-C5 ν N2-C7	1234	ν N2-C5 ν N2-C7	1243	ν N2-C6 β C14-H34 ν C7-C14	1248	ν N2-C5 ν N2-C7	1242	ν N2-C6
1228m		1223sh	1228	ν N2-C6			1228	ρ' CH ₃ (C12) ρ' CH ₃ (C11)	1224	ν N3-C12	1226	ρ CH ₃ (C12)	1238	ρ CH ₃ (C12)
1218sh	1208s	1218w	1217	ν N2-C7	1216	ρ' CH ₃ (C12)			1221	ν N2-C7	1216	ρ' CH ₃ (C11)	1223	ν N2-C7
1218sh	1208s	1209sh			1210	ν N2-C6	1211	ν N2-C7 β C15-H35 ρ CH ₃ (C11) δ C8C4N3						
1170w	1189vs	1209sh	1187	ν N3-C11	1187	ρ' CH ₃ (C11)	1181	ρ CH ₃ (C11) δ C8C4N3			1178	ρ' CH ₃ (C12)	1200	ρ' CH ₃ (C11)
1170w	1189vs	1171sh							1166	β C17-H37	1167	β C17-H37	1172	ρ CH ₃ (C11)
1162sh	1167sh	1164m	1153	β C18-H38 β C20-H40	1156	β C17-H37	1155	β C17-H37	1164	ρ CH ₃ (C11) ρ' CH ₃ (C12)	1166	β C18-H38 β C20-H40	1167	β C17-H37
		1156sh	1151	β C17-H37	1155	β C18-H38 β C20-H40	1153	β C18-H38	1163	β C18-H38	1157	ρ' CH ₃ (C11) ρ CH ₃ (C11)	1164	β C18-H38 β C20-H40
1142w			1143	ρ CH ₃ (C11) ρ CH ₃ (C12)	1141	ρ' CH ₃ (C12)	1138	ρ CH ₃ (C12)	1137	β C20-H40	1138	β C19-H39	1138	ν C15-C19
1128m		1129sh	1126	β C19-H39 β C20-H40	1128	ν C15-C19	1128	β C19-H39 β C20-H40	1120	β C19-H39 β C20-H40	1121	ν C15-C19	1121	ν C16-C20
1106w	1117sh	1118m	1109	ν C15-C19	1111	ν C16-C20 ν C15-C19	1111	ν C16-C20	1111	ρ CH ₃ (C8)	1100	ρ CH ₃ (C8) ν N2-C5		
1091sh	1103m	1105m	1097	ρ' CH ₃ (C8)			1094	ρ' CH ₃ (C8)	1103	ρ CH ₃ (C11) ρ' CH ₃ (C12)	1095	ρ CH ₃ (C8)	1107	ρ CH ₃ (C8)
1091sh	1103m	1105m	1084	ρ CH ₃ (C12) ρ CH ₃ (C11)	1089	ν N2-C5			1089	ν N2-C5 ν C7-C10			1091	ν N2-C5
1082sh	1075sh	1088sh	1080	ν N2-C5 ν C9-S1	1084	ν N2-C5	1082	ν N2-C5	1079	ρ' CH ₃ (C8)			1079	ν C4-C8
1066vw	1066sh		1073	ν C4-C8			1069	ν C4-C8	1067	ν C4-C8	1072	ν C4-C8		
1059vw		1058sh	1060	ρ' CH ₃ (C11)	1057	ρ' CH ₃ (C8)	1052	β R ₁ (A3)			1057	β R ₁ (A3)	1057	ρ' CH ₃ (C12)
1048sh			1047	β R ₁ (A1)	1054	β R ₁ (A3)	1050	ρ CH ₃ (C11)	1052	β R ₁ (A3)			1053	β R ₁ (A3)
1043m	1040sh	1044sh	1043	β R ₁ (A1)	1048	β R ₁ (A3)	1048	β R ₁ (A1)	1048	β R ₁ (A1)	1051	β R ₁ (A1)	1051	β R ₁ (A1)
1034m		1027vs	1030	ρ' CH ₃ (C12) ν N3-C11	1023	ν C17-C19 ρ CH ₃ (C12)	1040	β R ₁ (A3)	1036	ρ' CH ₃ (C11) ν N3-C11	1031	ν C17-C19	1034	ν C4-C8 β R ₁ (A3)
1034m		1027vs	1023	ν C17-C19	1020	ρ CH ₃ (C11) ρ CH ₃ (C12)			1033	ν C17-C19 ν C15-C19	1029	ν C18-C20 ν C16-C20	1033	ν C17-C19 ν C18-C20
1034m		1027vs	1021	ν C18-C20 ν C16-C20	1019	ν C18-C20 ν C16-C20	1024	ν C17-C19	1031	ν C18-C20 ν C16-C20	1025	ρ CH ₃ (C11)	1032	ν C18-C20 ν C17-C19 ν C15-C19
1009sh	1012s	1008sh			1015	ν C4-C8 ν C4-C5	1021	ν C18-C20 ν C15-C19						
1005w	1012s 987s	1008sh 996sh			987		988				1006 981	ρ' CH ₃ (C8)	1002	ν N3-C11

Table 15 (continued)

Experimental			B3LYP/6-31G* Method ^a												
			S(-)-PTZ						R(+)-PTZ						
			Free base		Cationic		Hydrochloride		Free base		Cationic		Hydrochloride		
IR ^c	IR ^d	Raman ^e	SQM ^b	Assignments ^a	SQM ^b	Assignments ^a	SQM ^b	Assignments ^a	SQM ^b	Assignments ^a	SQM ^b	Assignments ^a	SQM ^b	Assignments ^a	
						γ C19-H39 γ C17-H37		ν N3-C11 ν N3-C12				γ C19-H39 γ C17-H37 γ C20-H40			
988vw			973	γ C18-H38 γ C20-H40									980		
976w		971vw	971	γ C17-H37	986	γ C20-H40	976	γ C20-H40 γ C18-H38	968	ν N3-C12 ν N3-C11				971	γ C17-H37
							975	γ C19-H39 γ C17-H37	964	γ C17-H37					
957sh	955s		957	ν N3-C12					963	γ C18-H38	958	ν N3-C11 ν N3-C12	965	γ C20-H40 γ C18-H38	
950w		949vw			949	ν N3-C11 ν N3-C12									
935sh	941sh		935	γ C16-H36	943	γ C15-H35	937	γ C15-H35			937	γ C15-H35	939	ρ CH ₃ (C8)	
930w	930sh		934	γ C15-H35	941	γ C16-H36 γ C18-H38	936	γ C16-H36	928	γ C15-H35 γ C13-H33	930	γ C16-H36 γ C18-H38	932	γ C15-H35	
924sh		929w			924	ρ CH ₃ (C8)	928	ν N3-C4 ρ CH ₃ (C8)	923	γ C16-H36	928	ρ CH ₃ (C8) γ C15-H35	922	γ C16-H36	
902w	893m	917sh	915	ρ CH ₃ (C8)			918	ρ CH ₃ (C8)	920	γ C15-H35			915	ν N3-C12	
884vw	893m				875	ν N3-C4			866	ν C4-C5	873	ν C4-C5	867	γ C13-H33 ν C4-C5	
874vw		873sh	854	γ C13-H33	856	γ C13-H33	862	ν C4-C5			861	γ C13-H33			
859w	856s	856w	851	γ C14-H34	854	γ C14-H34	853	γ C14-H34	856	γ C13-H33	854	γ C14-H34	857	γ C13-H33 γ C15-H35	
852w	832sh	842sh	847	ν C4-C5	852	γ C14-H34 γ C16-H36	850	γ C13-H33	852	γ C14-H34	844	ν N3-C11 ν N3-C12	850	γ C14-H34	
807vw	817sh	808m	803	τ wCH ₂	808	τ wCH ₂	813	τ wCH ₂	816	τ wCH ₂	811	τ wCH ₂	813	τ wCH ₂	
778sh	775sh	775sh	778	β R ₂ (A1)	774	β R ₂ (A1)	777	β R ₂ (A1)	794	δ C5C4N3	787	ν N3-C4	803	ν N3-C4 δ C5C4N3	
759vs	758s	761w	752	γ C19-H39	756	γ C19-H39 γ C17-H37	754	ν N3-C4	760	ν N3-C4	760	γ C19-H39 γ C17-H37	762	β R ₂ (A1)	
759vs	758s	761w							756	γ C19-H39	755	γ C20-H40 γ C14-H34	757	γ C19-H39	
759vs	758s	754sh	751	γ C20-H40	751	γ C20-H40 γ C18-H38	752	γ C20-H40	751	γ C20-H40			752	γ C20-H40 γ C18-H38	
752sh	742sh		745	γ C20-H40 γ C19-H39			746	γ C20-H40 γ C18-H38			747	ν N3-C4			
734m		737sh	722	τ R ₁ (A1)	723	τ R ₁ (A3) τ R ₁ (A1)	722	τ R ₁ (A1)	723	τ R ₁ (A3)	722	τ R ₁ (A3)	722	τ R ₁ (A3)	
		729m			720	τ R ₁ (A1)									
712vw	718m		714	τ R ₁ (A3)	713	τ R ₁ (A3)	714	τ R ₁ (A3)	716	τ R ₁ (A1)	716	τ R ₁ (A1)	715	τ R ₁ (A1)	
695w	687m	688sh	686	β R ₂ (A3)	683	τ R ₁ (A3)	686	β R ₂ (A3)	688	β R ₂ (A3)	685	τ R ₁ (A3)	688	τ R ₁ (A3)	
						τ R ₁ (A1)					τ R ₁ (A1)			τ R ₁ (A1)	
675w	655m	672s	676	β R ₃ (A1)	675	β R ₃ (A1) β R ₂ (A3)	677	β R ₃ (A1)	677	β R ₃ (A1)	676	β R ₃ (A1)	677	β R ₃ (A1) β R ₂ (A3)	
	646s	616vw	623	β R ₃ (A3)	619	β R ₃ (A3)	631	β R ₃ (A3)	623	β R ₃ (A3)	619	β R ₃ (A3)	622	β R ₃ (A3)	
	613w	594vw	609	β R ₂ (A1)	611	β R ₂ (A1)	613	β R ₂ (A1)	605	β R ₂ (A1) β R ₁ (A2)	601	β R ₁ (A2) β R ₂ (A1)	604	β R ₂ (A1) β R ₁ (A2)	
	567s	540w	539	τ R ₁ (A2) τ R ₃ (A1)	534	τ R ₃ (A1)	546	τ R ₂ (A3) τ R ₁ (A2)	537	τ R ₁ (A2) τ R ₃ (A1)	532	τ R ₁ (A2) τ R ₃ (A1)	538	τ R ₁ (A2) γ N2-C5	
			524	β R ₁ (A2)	526	β R ₁ (A2)	530	β R ₁ (A2)	524	τ R ₃ (A1)	519	τ R ₃ (A1)	525	τ R ₃ (A1)	
	510vw	518sh	520	τ R ₃ (A3)	517	τ R ₃ (A3)	520	τ R ₃ (A3) τ R ₃ (A1)	522	τ R ₃ (A3)	514	τ R ₃ (A3)	520	τ R ₃ (A3)	

Table 15 (continued)

Experimental			B3LYP/6-31G* Method ^a											
			S(-)-PTZ						R(+)-PTZ					
			Free base		Cationic		Hydrochloride		Free base		Cationic		Hydrochloride	
IR ^c	IR ^d	Raman ^e	SQM ^b	Assignments ^a	SQM ^b	Assignments ^a	SQM ^b	Assignments ^a	SQM ^b	Assignments ^a	SQM ^b	Assignments ^a	SQM ^b	Assignments ^a
	486sh	508w	502	δC8C4N3			497	τR ₃ (A1)	490	δC8C4N3	494	δC5C4C8 δC11N3C12	503	δC5C4C8 νH41-Cl42
	486sh	508w			486	δC4N3C12 τR ₂ (A1)	489	δC8C4N3	479	δC5C4C8			475	δC11N3C12 δC4N3C11
	482s	479sh			473	δC8C4N3					466	δC11N3C12 δC4N3C11	471	δC4N3C12
		470w	451	δC4N3C11	444	τR ₂ (A3)	447	τR ₂ (A3) τR ₂ (A1)	445	τR ₂ (A3) τR ₂ (A1)			441	τR ₂ (A3)
	440s	440sh	439	δC11N3C12					439	τR ₂ (A3) ButtC6-C9	438	τR ₂ (A3)		
			435	τR ₂ (A3)	432	τR ₂ (A1)	434	τR ₂ (A1)	434	τR ₂ (A1)	434	τR ₂ (A1)	434	τR ₂ (A1)
	423sh	423m	426	τR ₂ (A1) νC10-S1	427	νC9-S1 νC10-S1	429	νC9-S1	427	νC9-S1 νC10-S1	427	νC10-S1 νC9-S1 βR ₂ (A3)	429	νC10-S1 νC9-S1
	423sh	423m	421	δC5C4N3	417	δC11N3C12	424	νC10-S1			418	δC8C4N3 δC4N3C12		
	392w	394sh	402	βR ₂ (A2) βR ₃ (A2)	401	βR ₂ (A2)	404	βR ₂ (A2)	407	βR ₂ (A2) βN2-C5	402	βR ₂ (A2)	407	βR ₂ (A2)
	392w	394sh									382	δC5C4C8	395	δC5C4C8
	370w	370sh	360	γN2-C5			375	δC11N3C12	379	δC4N3C11			377	δC8C4N3
	357sh	357sh	352	δC5C4C8	358	βR ₃ (A2)	356	βR ₃ (A2) δC5C4C8	356	γN2-C5 βR ₃ (A2)	357	βR ₃ (A2)	356	βR ₃ (A2)
	357sh	357sh			349	δC5C4C8			346	δC4N3C12	347	δC4N3C12 δC4N3C11		
		340sh 337s	333	βR ₂ (A2)	331	τR ₂ (A3)	332 325	τR ₂ (A3) βN2-C5	337	τR ₂ (A3)	336	τR ₂ (A3)	340	τR ₂ (A3) γN2-C5 βN2-C5
	320sh	325sh	319	τR ₂ (A3) δC11N3C12	315	βN2-C5							318	βN2-C5
	303m	294vw							302	δC11N3C12	305	βN2-C5 δC5C4N3		
	278sh		281	βN2-C5 δC4N3C12			288	δC4N3C12 δC4N3C11	280	τR ₂ (A2)				
	278sh				273	δC4N3C12	272	τR ₂ (A2)	272	τWCH ₃ (C8)	273	τR ₂ (A2)	284	τR ₂ (A2)
	245sh		266	τR ₂ (A2)	263	δC4N3C11					257	τWCH ₃ (C8)	267	τWCH ₃ (C8)
	235m						232	νH41-Cl42	233	ButtC7-C10			232	ButtC7-C10 ButtC6-C9
	235m		227	ButtC6-C9 ButtC7-C10	228	ButtC6-C9 ButtC7-C10	228	ButtC6-C9 ButtC7-C10						
					220	τWCH ₃ (C11)			225	τWCH ₃ (C11)	226	ButtC7-C10 ButtC6-C9	222	νH41-Cl42
	215s		211	τWCH ₃ (C11) τWCH ₃ (C12)	214	τWCH ₃ (C8)			213	τWCH ₃ (C12)	218	τWCH ₃ (C11)		
			209	τWCH ₃ (C12)			209	τWCH ₃ (C8)						
	204sh		203	τWCH ₃ (C11)					201	δN2C5C4	201	δN2C5C4	206	δN2C5C4
	195sh		194	τWCH ₃ (C8)	198	δN2C5C4	197	δN2C5C4					194	τWCH ₃ (C11)
	188sh				196	τWCH ₃ (C12)			188	τWCH ₃ (C11)				
							178	τWCH ₃ (C12)	177	τR ₂ (A2) τR ₁ (A2)	178	τR ₂ (A2) τWCH ₃ (C12)	180	τR ₂ (A2) τR ₁ (A2)
			155	τR ₁ (A2)	159	δC5C4N3	157	τR ₁ (A2) τR ₂ (A2)						

Table 15 (continued)

Experimental			B3LYP/6-31G* Method ^a												
			S(-)-PTZ						R(+)-PTZ						
			Free base		Cationic		Hydrochloride		Free base		Cationic		Hydrochloride		
IR ^c	IR ^d	Raman ^e	SQM ^b	Assignments ^a	SQM ^b	Assignments ^a	SQM ^b	Assignments ^a	SQM ^b	Assignments ^a	SQM ^b	Assignments ^a	SQM ^b	Assignments ^a	
							140	$\tau R_1(A2)$			164	$\tau wCH_3(C12)$	154	$\tau wCH_3(C12)$	
									144	$\tau R_1(A2)$	143	$\tau R_1(A2)$	143	$\tau R_1(A2)$	
			136	$\tau R_3(A1)$	139	$\tau R_1(A2)$									
			118	$\tau R_3(A2)$	115	$\tau R_3(A2)$	119	$\tau R_3(A2)$	122	$\tau R_3(A2)$ $\tau R_3(A3)$	119	$\tau R_3(A2)$	119	$\tau R_3(A2)$	
							105	$\tau N3-H41$ $\delta N3H41Cl42$					83	$\delta N3H41Cl42$ $\rho' N3-H41$	
			80	$\tau N3-C4$			80	$\delta N3H41Cl42$						70	$\tau N3-C4$ $\tau N3-H41$
			62	$\tau R_2(A2)$ $\gamma N2-C5$	72	$\tau N3-C4$	66	$\tau N3-C4$	72	$\tau R_3(A2)$				62	$\tau N3-H41$
			54	$\tau R_2(A2)$ $\delta N2C5C4$	58	$\tau R_2(A2)$	57	$\tau R_2(A2)$	60	$\tau R_2(A2)$	61	$\gamma N2-C5$ $\tau wN2-C5$			
			42	$\gamma N2-C5$ $\tau wN2-C5$	52	$\gamma N2-C5$ $\tau N3-C4$ $\tau C4-C5$			47	$\tau N3-C4$	58	$\tau R_2(A2)$	54	$\tau R_2(A2)$ $\tau R_2(A2)$	
					36	$\tau C4-C5$	31	$\gamma N2-C5$	37	$\tau C4-C5$	35	$\tau C4-C5$	37	$\gamma N2-C5$ $\tau wN2-C5$	
			31	$\tau wN2-C5$ $\tau C4-C5$			27	$\tau N3-C4$ $\tau C4-C5$	27	$\tau wN2-C5$	32	$\tau N3-C4$ $\gamma N2-C5$	31	$\tau C4-C5$	
					24	$\gamma N2-C5$ $\tau wN2-C5$	21	$\tau C4-C5$ $\tau wN2-C5$			18	$\tau N3-C4$	18	$\tau N3-C4$	

Abbreviations: ν , stretching; β , deformation in the plane; γ , deformation out of plane; wag, wagging; τ , torsion; βR , deformation ring; τR , torsion ring; ρ , rocking; τw , twisting; δ , deformation; a, antisymmetric; s, symmetric; (A1), Ring 1.

^a This work.

^b From scaled quantum mechanics force field.

^c From Ref [66].

^d From Ref [10].

^e From Ref [10].

Table 16

Scaled internal force constants for the free base, cationic and hydrochloride species of S(-) and R(+)- promethazine in gas phase by using the B3LYP/6-31G* method compared with the corresponding to cyclizine.

Force constant	Promethazine ^a						Cyclizine ^b		
	S(-)			R(+)			Free base	Cationic	HCl/PCM
	Free base	Cationic	HCl	Free base	Cationic	HCl			
$f(\nu N-H)$		6.02	2.47		5.94	2.60		5.91	4.61
$f(\nu N-CH_3)$	4.67	3.92	4.25	4.70	3.94	4.94	4.85	4.06	4.33
$f(\nu C-N)$	4.97	4.65	4.82	5.05	4.74	4.96	4.54	4.13	4.19
$f(\nu CH_2)$	4.74	4.72	4.74	4.85	4.76	4.89	4.62	4.82	4.87
$f(\nu CH_2)$	4.82	4.83	4.85	4.90	4.94	4.95	4.69	5.06	5.07
$f(\nu C-H)_R$	5.11	5.11	5.11	5.18	5.19	5.19	5.15	5.17	5.18
$f(\nu C-H)$	4.73	4.82	4.81	4.45	4.90	4.78	4.31	4.44	4.74
$f(\nu C=C)$							6.50	6.50	6.46
$f(\nu C-C)$	3.40	3.57	3.65	3.70	3.56	3.69			
$f(\delta CH_2)$	0.78	0.79	0.79	0.81	0.82	0.81	0.74	0.73	0.73
$f(\delta CH_3)$	0.53	0.53	0.53	0.56	0.56	0.57	0.58	0.56	0.55

Units are mdy \AA^{-1} for stretching and mdy $\text{\AA} \text{rad}^{-2}$ for angle deformations.

^a This work.

^b From Ref. [9].

3.8. Force fields

Both S(-) and R(+)-PTZ enantiomers have evidenced differences in the positions of IR bands because differences in their geometrical parameters are observed. Hence, it is necessary to investigate if the harmonic force constants present some changes since these parameters are also strongly dependent of their structures. Hence, the force fields for all species of both forms are calculated in gas phase by using B3LYP/6-31G* level of theory. These parameters are compared in Table 16 with the reported for the three species of cyclizine [9]. In general, the force constants for the R(+)-PTZ enantiomer have higher values than the corresponding to the S(-) form. Comparing the $f(\nu N-H)$ force constants of all species, we observed that the cationic species of both forms of PTZ and cyclizine are higher than the hydrochloride ones because the presence of electronegative Cl atoms linked to H atoms generate an enlargement of N-H bonds with the consequent reduction of their $f(\nu N-H)$ force constants. Note that in hydrochloride cyclizine the presence of N-CH₃ group linked to two rings produces a higher value in its force constant (4.61 mdy \AA^{-1}), as compared with both forms of PTZ. Probably, for this same reason, the $f(\nu N-CH_3)$ force constants of free base and cationic species of cyclizine have higher values than the corresponding to PTZ. On the other hand, the hydrochloride species of R(+) has higher value than the other ones because the distances observed for both N-CH₃ groups are lower in the R(+) form than the S(-) one, as observed in Tables 3 and 4. Note that the $f(\nu C-H)$ force constants corresponding to the aromatic rings in general are higher in all species than the aliphatic ones and, moreover, these values are similar to those published for the species of diphenhydramine [8]. The remaining constants have similar values in the two compared species, as is observed in Table 16.

3.9. Ultraviolet-visible spectrum

The electronic spectra of free base, cationic and hydrochloride species of both S(-) and R(+)-PTZ enantiomers were predicted in aqueous solution with the TD-DFT method and the Gaussian program [55] by using the B3LYP/6-31G* level of theory. The experimental UV-Vis spectrum of a racemic mixture of hydrochloride species of both enantiomers in ethanol solution was taken from Ref. [68] where in each enantiomer it is observed one intense band at c. a. 250 nm and

where one of them is slightly most intense than the other one. In all theoretical spectra are observed one intense band, whose positions are respectively in free base, cationic and hydrochloride species of S(-) form at 247.0 (shoulder at 283.2 nm), 290.8 and 290.2 nm while and in the R(+) form the positions of those bands change at 245.7 (shoulder at 280.0 nm), 292.7 and 284.4 nm, respectively. The shifting of the bands observed in the experimental UV spectra from 250 to 290 nm, in relation to the theoretical ones, can be attributed to the different solvents. All UV spectra are compared in Fig. 11 with the corresponding experimental one. Here, it is evident that the free base species of both forms are protonated, as suggested by the shoulders at higher wavelengths and closer to the values for the cationic species. Also, the proximities between the maxima of both hydrochloride forms show that these species are as cationic species. Hence, these spectra evidence clearly the presence of both cationic S(-) and R(+) forms in solution. Obviously, the $\pi \rightarrow \pi^*$ transitions due to the C=C double bonds justify the intense bands observed in the experimental spectra, as supported by NBO calculations.

3.10. Electronic circular dichroism (ECD)

The experimental ECD spectrum of hydrobromide promethazine was taken from Ref [66] which shows two bands with opposite polarity, one of them with cotton effect and the other one positive. This ECD spectrum is similar to that recorded in the 190–240 nm region by Rub et al. in the study of interaction of gelatin with promethazine hydrochloride [64]. On the other hand, the predicted ECD spectra for the free base of R(+) shows one positive band while in the S(-) form one negative in the same position. In the same region, in the cationic species of R(+) form can be observed two bands one positive and other negative while in the S(-) form two bands negative. The hydrochloride species of S(-) and R(+) forms show one band positive and two negative in different positions, hence, these forms evidently are not present in the experimental spectrum in solution. Here, only the predicted ECD spectra in solution for the cationic species of both enantiomers present similarity with the experimental one, for which, both species are present in a racemic sample of hydrochloride promethazine in aqueous solution. Then, the two negative and positive bands observed in the experimental spectrum at 250 nm could be assigned to $\pi \rightarrow \pi^*$ transitions.

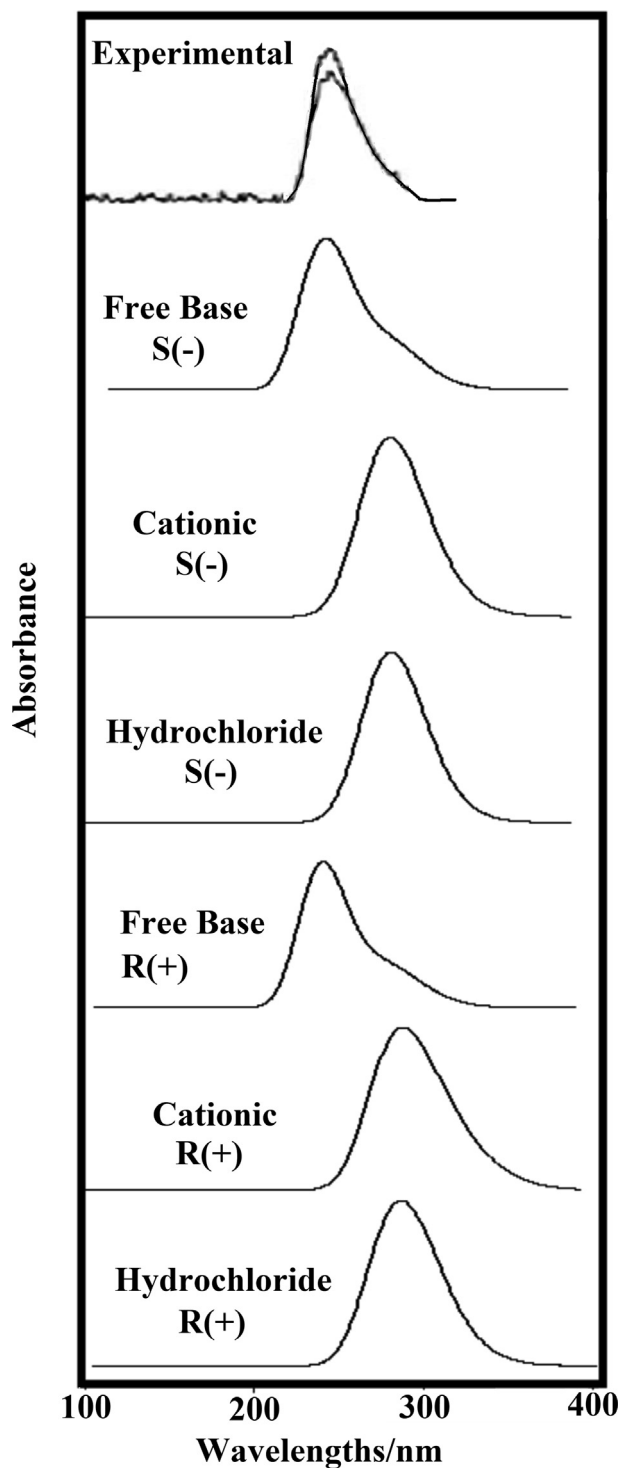


Fig. 11. Experimental electronic spectrum of hydrochloride promethazine in ethanol solution compared with the corresponding predicted for the free base, cationic and hydrochloride species of both S(-) and R(+) enantiomers in aqueous solution by using B3LYP/6-31G* level of theory.

4. Conclusions

In this work, the molecular structures of free base, cationic and hydrochloride species of both S(-) and R(+)- enantiomers of promethazine antihistaminic agent were theoretically studied in gas phase and in aqueous solution by using the hybrid B3LYP/6-31G* method. The initial structures of S(-) and R(+) enantiomers of PTZ hydrochloride were those

polymorphic forms 1 and 2 experimentally determined by X-ray diffraction. In solution, all species were optimized with the SCRF methodology by using the PCM and SD models. The corrected solvation energies (ΔG_s) by the total non-electrostatic terms and by zero point vibrational energy (ZPVE) were computed for all species showing the higher value the cationic species of R(+) form. The comparisons of geometrical parameters with the corresponding experimental ones have showed slight differences in the dihedral angles of both S(-) and R(+)-PTZ forms that later they are evidenced in the different vibrational assignments of their infrared and Raman spectra and in the calculated force constants. Here, the studied MK, Mulliken and NPA charges have evidenced variations in the three species of both enantiomers observing the higher MK charges on N2 atoms of the cationic species of R(+) species in the two media. The cationic and hydrochloride species present basically the same behaviours in the Mulliken charges where the lower values are observed on N2 atoms. The mapped surfaces MEP have clearly evidenced nucleophilic sites in the free base on the N3 and S1 atoms and in the hydrochloride species on the Cl atoms. The NBO and AIM studies reveal clearly that the hydrochloride species are most stable than the other two species of both forms and in both media and, in particular, the species of R(+)-PTZ evidence a slight higher stability than the S(-) one. The frontier orbitals studies show that the free base species of both forms in solution are more reactive than cyclizine. Higher electrophilicity indexes are observed in the cationic and hydrochloride species of PTZ than cyclizine while the cationic species of cyclizine have higher nucleophilicity index than both species of PTZ. The predicted infrared, Raman, UV-Visible and ECD have showed a reasonable concordance with the corresponding experimental available spectra. The presences of cationic species of both enantiomers are clearly supported by the infrared, Raman, UV-Vis and ECD spectra. The increase in the volume of cationic and hydrochloride species in solution could suggest the H bonds formation, as supported by AIM study. The force fields were computed by using the SQMFF approach and Molvib program which were used to perform the complete vibrational analysis. Here, the 114, 117 and 120 vibration normal modes expected for the free base, cationic and hydrochloride species were assigned and the force constants reported and compared with other reported from the literature.

Declarations

Author contribution statement

María Eugenia Manzur: Performed the experiments; Contributed reagents, materials, analysis tools or data.

Silvia A. Brandán: Conceived and designed the experiments; Performed the experiments; Analyzed and interpreted the data; Contributed reagents, materials, analysis tools or data; Wrote the paper.

Funding statement

This work was supported by grants from CIUNT Project N° 26/D608 (Consejo de Investigaciones, Universidad Nacional de Tucumán).

Competing interest statement

The authors declare no conflict of interest.

Additional information

No additional information is available for this paper.

References

- [1] S.A. Brandán, Why morphine is a molecule chemically powerful. Their comparison with cocaine, *Indian J. Appl. Res.* 7 (7) (2017) 511–528.

- [2] R.A. Rudyk, S.A. Brandán, Force field, internal coordinates and vibrational study of alkaloid tropane hydrochloride by using their infrared spectrum and DFT calculations, *Paripex - Indian J. Res.* 6 (8) (2017) 616–623.
- [3] D. Romani, S.A. Brandán, Vibrational analyses of alkaloid cocaine as free base, cationic and hydrochloride species based on their internal coordinates and force fields, *Paripex - Indian J. Res.* 6 (9) (2017) 587–602.
- [4] Iramain MA, AE Ledesma, S.A. Brandán, Analyzing the effects of halogen on properties of a halogenated series of R and S enantiomers analogues alkaloid cocaine-X, X=F, Cl, Br, I. *Paripex - Indian J. Res.* 6 (12) (2017) 454–463.
- [5] S.A. Brandán, Understanding the potency of heroin against morphine and cocaine, *IJSRM, Int. J. Soc. Res. Methodol.* 12 (2) (2018) 97–140.
- [6] R.A. Rudyk, M.A. Checa, K.A. Guzzetti, M.A. Iramain, S.A. Brandán, Behaviour of N-CH₃ group in tropane alkaloids and correlations in their properties, *IJSRM, Int. J. Soc. Res. Methodol.* 10 (4) (2018) 70–97.
- [7] R.A. Rudyk, M.A. Checa, C.A.N. Catalán, S.A. Brandán, Structural, FT-IR, FT-Raman and ECD spectroscopic studies of free base, cationic and hydrobromide species of scopolamine alkaloid, submitted to, *J. Mol. Struct.* 1180 (2018) 603–617.
- [8] Iramain MA, S.A. Brandán, Structural and vibrational properties of three species of anti-histaminic diphenhydramine by using DFT calculations and the SQM approach, *Chem. J.* 1 (1) (2018) 105–130.
- [9] María J. Márquez, Maximiliano A. Iramain, Silvia Antonia Brandán, *Ab-initio* and vibrational studies on free base, cationic and hydrochloride species derived from antihistaminic cyclizine agent, *IJSRM, Int. J. Soc. Res. Methodol.* 12 (2) (2018) 97–140.
- [10] M.C. Davies, J.S. Binns, C.D. Melia, P.J. Hendra, D. Bourgeois, S.P. Church, P.J. Stephenson, FT Raman spectroscopy of drugs in polymers, *Int. J. Pharm.* 66 (1990) 223–232.
- [11] Francisco J. Lara, Ana M. García-Campana, F. Al'es-Barrero, Juan M. Bosque-Sendra, Determination of thiazinamium, promazine and promethazine in pharmaceutical formulations using a CZE method, *Anal. Chim. Acta* 535 (2005) 101–108.
- [12] Sylwester Mazurek, Roman Zostak, Quantitative determination of diclofenac sodium in solid dosage forms by FT-Raman spectroscopy, *J. Pharm. Biomed. Anal.* 48 (2008) 814–821.
- [13] C.B. Page, S.B. Duffull, I.M. Whyte, G.K. Isbister, Promethazine overdose: clinical effects, predicting delirium and the effect of charcoal, *Q. J. Med.* 102 (2009) 123–131.
- [14] Ruchi Tiwari, Birendra Srivastava, Gaurav Tiwari, Awanik Rai, Extended release promethazine HCl using acrylic polymers by freeze-drying and spray-drying techniques: formulation considerations, *Braz. J. Pharma. Sci.* 45 (4) (2009) 829–840.
- [15] Sara Abalde-Cela, Paula Aldeanueva-Potel, Cintia Mateo-Mateo, Laura Rodríguez-Lorenzo, R.A. Alvarez-Puebla, M. Luis, Liz-Marzán, Surface-enhanced Raman scattering biomedical applications of plasmonic colloidal particles, *J. R. Soc. Interface* 7 (2010) S435–S450.
- [16] Charles J. Choi, Hsin-Yu Wu, Jonathan Weyhenmeyer, Sherine George, and Brian T. Cunningham, Nanodome Sensor Tubing for Monitoring of Intravenous Drug Infusion and Metabolites, 2011 11th IEEE International Conference on Nanotechnology Portland Marriott August 15-18, 2011, Portland, Oregon, USA.
- [17] Michael D. Hargreaves, Neil A. Macleod, Mark R. Smith, Darren Andrews, Stephen V. Hammond, Pavel Matousek, Characterisation of transmission Raman spectroscopy for rapid quantitative analysis of intact multi-component pharmaceutical capsules, *J. Pharm. Biomed. Anal.* 54 (2011) 463–468.
- [18] J. Choi Charles, Hsin-Yu Wu, Jonathan Weyhenmeyer, Sherine George, Brian T. Cunningham, Biochemical sensor tubing for point-of-care monitoring of intravenous drugs and metabolites, *Lab Chip* 3 (2012).
- [19] Georghie Borodi, Mihaela M. Pop, Oana Onija, Xenia Filip, Distinct disordered forms of promethazine hydrochloride: a case of intergrowth of polymorphic domains? *Cryst. Growth Des.* 12 (2012) 5846–5851.
- [20] Neha Maurya, Mehraj ud din Parray, Jitendra Kumar Maurya, Amit Kumar, Rajan Patel, Interaction of promethazine and adiphenine to human hemoglobin: a comparative spectroscopic and computational analysis, *Spectrochim. Acta A Mol. Biomol. Spectrosc.* 199 (2018) 32–42.
- [21] C. Cantisani, S. Ricci, T. Grieco, G. Paolino, V. Faina, E. Silvestri, S. Calvieri, Topical Promethazine Side Effects: Our Experience and Review of the Literature 2013, Hindawi Publishing Corporation, BioMed Research International, 2013, p. 9. Article ID 151509.
- [22] Sulaf Assi, Raw material identification using dual laser handheld Raman spectroscopy, *Eur. Pharma. Rev.* 18 (5) (2013) 25–31.
- [23] Wei Xie, Sebastian Schlücker, Medical applications of surface-enhanced Raman scattering, *Phys. Chem. Chem. Phys.* 15 (2013) 5329–5344.
- [24] Ying-Sing Li, Jeffrey S. Church, Raman spectroscopy in the analysis of food and pharmaceutical nanomaterials, *J. Food Drug Anal.* 22 (2014) 29–48.
- [25] Kenny Kong, Catherine Kendall, Nicholas Stone, Ioan Notingher, Raman spectroscopy for medical diagnostics-From in-vitro biofluid assays to in-vivo cancer detection, *Adv. Drug Deliv. Rev.* 89 (2015) 121–134.
- [26] Amrit Paudel, Dhara Raijada, Jukka Rantanen, Raman spectroscopy in pharmaceutical product design, *Adv. Drug Deliv. Rev.* 89 (2015) 3–20.
- [27] Gurvinder Singh Bumrah, Rakesh Mohan Sharma, Raman spectroscopy – basic principle, instrumentation and selected applications for the characterization of drugs of abuse, *Egypt. J. Food Sci* 6 (2016) 209–215.
- [28] Tawfik A. Saleh, Pharmaceutical characterization and detection using surface-enhanced Raman scattering, *Saleh. Int. Arch. Clin. Pharmacol.* 3 (2017) 7, 010.
- [29] P. Tarkkila, K. Torn, M. Tuominen, L. Lindgren, Premedication with promethazine and transdermal scopolamine reduces the incidence of nausea and vomiting after intrathecal morphine, *Acta Anaesthesiol. Scand.* 39 (7) (1995) 983–986.
- [30] C. Vidal Pan, A. González Quintela, P. Galdos Anuncibay, J. MateoVic, Topical promethazine intoxication, *Curr. Med. Res. Opin.* 28 (4) (2012) 623–642.
- [31] Promethazine should not be used for infants, *Die Pharmazie* 65 (5) (2010) 339–342.
- [32] M.R. Cohen, Frequency and severity of promethazine adverse event reports obligated the ISMP alert, *Jt. Comm. J. Qual. Patient Saf.* 36 (3) (2010) 143–144.
- [33] Y. Kai, O. Okamoto, S. Fujiwara, Fixed drug eruption caused by three unrelated drugs: promethazine, pethidine and omeprazole, *Clin. Exp. Dermatol.* 36 (7) (2011) 755–758.
- [34] A.D. Becke, Density-functional exchange-energy approximation with correct asymptotic behavior, *Phys. Rev. A* 38 (1988) 3098–3100.
- [35] C. Lee, W. Yang, R.G. Parr, Development of the Colle-Salvetti correlation-energy formula into a functional of the electron density, *Phys. Rev. B* 37 (1988) 785–789.
- [36] S. Miertus, E. Scrocco, J. Tomasi, Electrostatic interaction of a solute with a continuum, *Chem. Phys.* 55 (1981) 117–129.
- [37] J. Tomasi, J. Persico, Molecular interactions in solution: an overview of methods based on continuous distributions of the solvent, *Chem. Rev.* 94 (1994) 2027–2094.
- [38] A.V. Marenich, C.J. Cramer, D.G. Truhlar, Universal solvation model based on solute electron density and a continuum model of the solvent defined by the bulk dielectric constant and atomic surface tensions, *J. Phys. Chem. B* 113 (2009) 6378–6396.
- [39] P. Pulay, G. Fogarasi, G. Pongor, J.E. Boggs, A. Vargha, Combination of theoretical *ab initio* and experimental information to obtain reliable harmonic force constants. Scaled quantum mechanical (QM) force fields for glyoxal, acrolein, butadiene, formaldehyde, and ethylene, *J. Am. Chem. Soc.* 105 (1983) 7073.
- [40] a) G. Rauhut, P. Pulay, Transferable scaling factors for density functional derived vibrational force fields, *J. Phys. Chem. B* 99 (1995) 3093–3100; b) Correction G. Rauhut, P. Pulay, *J. Phys. Chem.* 99 (1995) 14572.
- [41] Available from. DL- 3,4- Methylenedioxyamphetamine, Spectra BASE, <https://spectrabase.com/spectrum/41WjF312JuZ>.
- [42] T. Sundius, Scaling of *ab-initio* force fields by MOLVIB, *Vib. Spectrosc.* 29 (2002) 89–95.
- [43] R.G. Parr, R.G. Pearson, Absolute hardness: companion parameter to absolute electronegativity, *J. Am. Chem. Soc.* 105 (1983) 7512–7516.
- [44] J.-L. Brédas, Mind the gap!, *Mater. Horizons* 1 (2014) 17–19.
- [45] D. Romani, S.A. Brandán, M.J. Márquez, M.B. Márquez, Structural, topological and vibrational properties of an isothiazole derivatives series with antiviral activities, *J. Mol. Struct.* 1100 (2015) 279–289.
- [46] D. Romani, S. Tsuchiya, M. Yotsu-Yamashita, S.A. Brandán, Spectroscopic and structural investigation on intermediates species structurally associated to the tricyclic bisguanidine compound and to the toxic agent, saxitoxin, *J. Mol. Struct.* 1119 (2016) 25–38.
- [47] E. Romano, M.V. Castillo, J.L. Pergomet, J. Zinczuk, S.A. Brandán, Synthesis, structural and vibrational analysis of (5,7-Dichloro-quinolin-8-yloxy) acetic acid, *J. Mol. Struct.* 1018 (2012) 149–155.
- [48] F.E. Chain, M.F. Ladetto, A. Grau, C.A.N. Catalán, S.A. Brandán, Structural, electronic, topological and vibrational properties of a series of N-benzylamides derived from Maca (*Lepidium meyenii*) combining spectroscopic studies with ONION calculations, *J. Mol. Struct.* 1105 (2016) 403–414.
- [49] F. Chain, M.A. Iramain, A. Grau, C.A.N. Catalán, S.A. Brandán, Evaluation of the structural, electronic, topological and vibrational properties of N-(3,4-dimethoxybenzyl)-hexadecanamide isolated from Maca (*Lepidium meyenii*) using different spectroscopic techniques, *J. Mol. Struct.* 1119 (2016) 25–38.
- [50] M. Minteguiga, E. Dellacassa, M.A. Iramain, C.A.N. Catalán, S.A. Brandán, A structural and spectroscopic study on carquejol, a relevant constituent of the medicinal plant *Baccharis trimera* (Less.) DC. (Asteraceae), *J. Mol. Struct.* 1150 (2017) 8–20.
- [51] M.A. Iramain, L. Davies, S.A. Brandán, Structural and spectroscopic differences among the Potassium 5-hydroxypentanoiltrifluoroborate salt and the furoyl and isonicotinoyl salts, *J. Mol. Struct.* 1176 (2019) 718–728.
- [52] N. Issaoui, H. Ghalla, S.A. Brandán, F. Bardak, H.T. Flakus, A. Atac, B. Oujia, Experimental FTIR and FT-Raman and theoretical studies on the molecular structures of monomer and dimer of 3-thiopheneacrylic acid, *J. Mol. Struct.* 1135 (2017) 209–221.
- [53] M. Minteguiga, E. Dellacassa, M.A. Iramain, C.A.N. Catalán, S.A. Brandán, FT-IR, FT-Raman, UV-Vis, NMR and structural studies of Carquejyl Acetate, a component of the essential oil from *Baccharis trimera* (Less.) DC. (Asteraceae), submitted to, *J. Mol. Struct.* (2018).
- [54] A.B. Nielsen, A.J. Holder, Gauss View 3.0, User's Reference, GAUSSIAN Inc., Pittsburgh, PA, 2000–2003.
- [55] M.J. Frisch, G.W. Trucks, H.B. Schlegel, G.E. Scuseria, M.A. Robb, J.R. Cheeseman, G. Scalmani, V. Barone, B. Mennucci, G.A. Petersson, H. Nakatsuji, M. Caricato, X. Li, H.P. Hratchian, A.F. Izmaylov, J. Bloino, G. Zheng, J.L. Sonnenberg, M. Hada, M. Ehara, K. Toyota, R. Fukuda, J. Hasegawa, M. Ishida, T. Nakajima, Y. Honda, O. Kitao, H. Nakai, T. Vreven, J.A. Montgomery Jr., J.E. Peralta, F. Ogliaro, M. Bearpark, J.J. Heyd, E. Brothers, K.N. Kudin, V.N. Staroverov, R. Kobayashi, J. Normand, K. Raghavachari, A. Rendell, J.C. Burant, S.S. Iyengar, J. Tomasi, M. Cossi, N. Rega, J.M. Millam, M. Klene, J.E. Knox, J.B. Cross, V. Bakken, C. Adamo, J. Jaramillo, R. Gomperts, R.E. Stratmann, O. Yazyev, A.J. Austin, R. Cammi, C. Pomelli, J.W. Ochterski, R.L. Martin, K. Morokuma, V.G. Zakrzewski, G.A. Voth, P. Salvador, J.J. Dannenberg, S. Dapprich, A.D. Daniels, O. Farkas, J.B. Foresman, J.V. Ortiz, J. Cioslowski, D.J. Fox, Gaussian, Inc., Wallingford CT, 2009.
- [56] P. Ugliengo, Moldraw Program, University of Torino, Dipartimento Chimica IFM, Torino, Italy, 1998.
- [57] B.H. Besler, K.M. Merz Jr., P.A. Kollman, Atomic charges derived from demiemperical methods, *J. Comput. Chem.* 11 (1990) 431–439.

- [58] E.D. Glendening, J.K. Badenhoop, A.D. Reed, J.E. Carpenter, F. Weinhold, NBO 3.1, Theoretical Chemistry Institute, University of Wisconsin, Madison, WI, 1996.
- [59] R.F.W. Bader, *Atoms in Molecules, A Quantum Theory*, Oxford University Press, Oxford, 1990.
- [60] F. Biegler-Köning, J. Schönbohm, D. Bayles, AIM2000; a program to analyze and visualize atoms in molecules, *J. Comput. Chem.* 22 (2001) 545.
- [61] G. Keresztury, S. Holly, G. Besenyi, J. Varga, A.Y. Wang, J.R. Durig, Vibrational spectra of monothiocarbamates-II. IR and Raman spectra, vibrational assignment, conformational analysis and *ab initio* calculations of *S*-methyl-*N,N*-dimethylthiocarbamate *Spectrochim. Acta* 49A (1993) 2007–2026.
- [62] D. Michalska, R. Wysokinski, The prediction of Raman spectra of platinum(II) anticancer drugs by density functional theory, *Chem. Phys. Lett.* 403 (2005) 211–217.
- [63] R. Lazny, A. Ratkiewicz, A. Nodzewska, A. Wymimko, L. Siergiejczyk, Determination of the *N*-methyl stereochemistry in tropane and granatane derivatives in solution: a computational and NMR spectroscopic study, *Tetrahedron Lett.* (2012).
- [64] M.A. Rub, A.M. Asiri, J.M. Khan, R.H. Khan, Kabir-ud Din, Interaction of gelatin with promethazine hydrochloride: conductimetry, tensiometry and circular dichroism studies, *J. Mol. Struct.* 1050 (2013) 35–42.
- [65] N.S. Bohloko, Development and Formulation of an Intranasal Dosage Form for Cyclizine Hydrochloride, Doctoral Thesis, Faculty of Health Sciences at the Department of Pharmaceutics, Potchefstroom University for Christian Higher Education, Potchefstroom, 2003.
- [66] Available from: <http://webbook.nist.gov/chemistry>.
- [67] E. Romano, L. Davies, S.A. Brandán, Structural properties and FTIR-Raman spectra of the anti-hypertensive clonidine hydrochloride agent and their dimeric species, *J. Mol. Struct.* 1133 (2017) 226–235.
- [68] F.G. Sánchez, A. Navas Díaz, E. Sánchez Torreño, A. Aguilar, I. Medina Lama, M. Algarra, Determination of enantiomeric excess by chiral liquid chromatography without enantiomerically pure starting standards, *Biomed. Chromatogr.* (2012).